AFRL-VS-HA-TR-2004-1030

# ANALYSIS AND SIMULATION OF CAVITY-DECOUPLELD CHEMICAL EXPLOSIONS


J. L. Stevens
N. Rimer
H. XU
J. R. Murphy
B. W. Barker
E. Bailey
C. Lindholm
S. Gibbons
F. Rindal
T. Kvaerna
I. Kitov

Science Applications International Corporation
10260 Campus Point Drive
San Diego, CA 92121-1578



24 October 2003

Scientific Report No. 2




APPROVED FOR PUBLIC RELEASE; DISTRIBUTION UNLIMITED



AIR FORCE RESEARCH LABORATORY
Space Vehicles Directorate
29 Randolph Rd
AIR FORCE MATERIEL COMMAND
Hanscom AFB, MA 01731-3010

This technical report has been reviewed and is approved for publication.

| /SIGNED/ | /SIGNED/ |
|---|---|
| ROBERT RAISTRICK | ROBERT BELAND |
| Contract Manager | Branch Chief |

This document has been reviewed by the ESC Public Affairs Office and has been approved for release to the National Technical Information Service (NTIS).

Qualified requestors may obtain additional copies from the Defense Technical Information Center (DTIC). All others should apply to the NTIS.

If your address has changed, if you with to be removed from the mailing list, or if the addressee is no longer employed by your organization, please notify AFRL/VSIM, 29 Randolph Rd., Hanscom AFB, MA 01731-3010. This will assist us in maintaining a current mailing list.

Do not return copies of this report unless contractual obligations or notices on a specific document require that it be returned.

# REPORT DOCUMENTATION PAGE

*Form Approved*
*OMB No. 0704-0188*



| 1. REPORT DATE *(DD-MM-YYYY)* | 2. REPORT TYPE | 3. DATES COVERED *(From - To)* |
|---|---|---|
| 19-10-2003 | SCIENTIFIC REPORT # 2 | 1 Oct 02 - 30 Sep 03 |

**4. TITLE AND SUBTITLE**
Analysis and Simulation of Cavity-Decoupled Chemical Explosions

**5a. CONTRACT NUMBER**
DTRA01-01-C-0069

**5b. GRANT NUMBER**

**5c. PROGRAM ELEMENT NUMBER**

**6. AUTHOR(S)**
J.L. Stevens, N. Rimer, H. Xu, J.R. Murphy, B.W. Barker, E. Bailey, C. Lindholm*, S. Gibbons*, F. Rindal*, T. Kvaerna*, and I. Kitov**

**5d. PROJECT NUMBER**
DTRA

**5e. TASK NUMBER**
OT

**5f. WORK UNIT NUMBER**
A1

**7. PERFORMING ORGANIZATION NAME(S) AND ADDRESS(ES)**
Science Applications International Corporation
10260 Campus Point Drive
San Diego, CA 92121-1578

**8. PERFORMING ORGANIZATION REPORT NUMBER**
SAIC 03/2050

**9. SPONSORING / MONITORING AGENCY NAME(S) AND ADDRESS(ES)**
Air Force Research Laboratory
29 Randolph Road
Hanscom AFB MA 01731-3010

**10. SPONSOR/MONITOR'S ACRONYM(S)**
AFRL/VSBYE

**11. SPONSOR/MONITOR'S REPORT NUMBER(S)**
AFRL-VS-HA-TR-2004-1030

**12. DISTRIBUTION / AVAILABILITY STATEMENT**
Approved For Public Release; Distribution Unlimited.

**13. SUPPLEMENTARY NOTES**
*NORSAR, Kjeller, NORWAY
**Institute for the Dynamics of the Geospheres, Academy of Sciences, Moscow, Russia

**14. ABSTRACT**
We analyze data from two sets of decoupled chemical explosions. NORSAR has obtained data from seven decoupled chemical explosions conducted from 1987-2002 in Alvdalen, Sweden, recorded both in he near field and on regional seismic stations NORES, HAGFORS, and NORSAR. The explosions were conducted in three granite chambers at a depth of approximately 100 meters in chambers with volumes of 200, 300 and 1000 m and yields ranging from 2500 kg to 10,000 kg. The smallest explosion in the largest chamber is almost fully decoupled while the other explosions are partially coupled, overdriven by up to a factor of 25. The data show that decoupling remains fairly constant for overdrive up to about a factor of 10, then decreases rapidly at higher yields. 1D and 3D simulations of these explosions are performed to model the data. IDG has digitized a set of surface seismic data recorded from a series of Soviet high-explosive cavity decoupling tests conducted in a mine in Kirghizia in the summer of 1960.

**15. SUBJECT TERMS**
Seismic discrimination  Seismic sources  Yield

| 16. SECURITY CLASSIFICATION OF: | | | 17. LIMITATION OF ABSTRACT | 18. NUMBER OF PAGES | 19a. NAME OF RESPONSIBLE PERSON |
|---|---|---|---|---|---|
| a. REPORT | b. ABSTRACT | c. THIS PAGE | | | Robert Raistrick |
| UNCLAS | UNCLAS | UNCLAS | SAR | | 19b. TELEPHONE NUMBER *(include area code)* 781 377-3726 |

## TABLE OF CONTENTS

## ABSTRACT

We analyze data from two sets of decoupled chemical explosions. NORSAR has obtained data from seven decoupled chemical explosions conducted from 1987-2002 in Älvdalen, Sweden, recorded both in the near field and on regional seismic stations NORES, HAGFORS, and NORSAR. The explosions were conducted in three granite chambers at a depth of approximately 100 meters in chambers with volumes of 200, 300 and 1000 $m^3$ and yields ranging from 2500 kg to 10,000 kg. The smallest explosion in the largest chamber is almost fully decoupled, while the other explosions are partially coupled, overdriven by up to a factor of 25. The data show that decoupling remains fairly constant for overdrive up to about a factor of 10, then decreases rapidly at higher yields. 1D and 3D simulations of these explosions are performed to model the data. IDG has digitized a set of surface seismic data recorded from a series of Soviet high-explosive cavity decoupling tests conducted in a mine in Kirghizia in the summer of 1960. These decoupled tests were carried out in a variety of mined cavities in limestone with the objectives of assessing the dependence of cavity decoupling effectiveness on cavity volume, cavity shape, and charge emplacement geometry. New data from these tests at distances of 5 and 10 km from the source augment earlier data from near field records of these explosions, allowing the frequency dependence of the decoupling factor to be measured. The decoupled tests conducted in the center of the cavities show low frequency chemical decoupling factors in the range 20-30, while that conducted 1 m from the wall of the 4.92 m radius cavity is about a factor of two smaller, indicating increased seismic coupling associated with nonlinear response of the cavity wall. Decoupling factors decrease to less than 10 at the high frequency.

## LIST OF FIGURES

## LIST OF TABLES

## PREFACE

The explosions discussed in section 3 of this report were conducted in a cooperative effort between the Norwegian Defense Building and Infrastructure Agency (Forsvarsbygg), Defense Science & Technology Agency (DSTA) of Singapore and the Swedish Defense Research Agency. The lead agency of the large scale tests, DSTA, and the other participants, kindly provided the data. We thank them for their support and for the use of their data.

# 1. EXECUTIVE SUMMARY

The objective of this project is to improve our capability to predict quantitatively the decoupling effectiveness of underground cavities in a variety of realistic configurations. This is being accomplished by expanding the existing decoupling data set with data that have recently become available from Russian and Swedish decoupled chemical explosions, and by performing data analysis and numerical modeling of this data set. This is a joint project of Science Application International Corporation (SAIC), the Russian Institute for the Dynamics of the Geospheres (IDG), and NORSAR.

Although cavity decoupling has been the subject of extensive study over a period of nearly 40 years, there is still considerable quantitative uncertainty in the decoupling factor – the ratio of coupled to decoupled seismic signal that can be achieved under different conditions. This uncertainty comes from three sources – first, there is only a limited amount of decoupled data available; second, there is considerable uncertainty in the low pressure equation of state used in numerical modeling of decoupled explosions; and third, there has been only a limited investigation of the effectiveness of decoupling by nonspherical cavities. In this report, we analyze and model two data sets provided by NORSAR and IDG. Our primary interest is to investigate:

1) the decoupling effectiveness of the rectangular chamber in granite for a range of partially coupled yields; and

2) the amplitude and frequency dependence of decoupling in the limestone cavity experiments.

NORSAR has obtained data from seven decoupled chemical explosions in Sweden. The explosions were conducted from 1987-2002 in Älvdalen, Sweden. The explosions were well recorded by the NORES, HAGFORS, and NORSAR arrays, except for the last explosion, which occurred shortly after NORES was damaged by lightning. NORSAR participated in the explosions during the summer of 2001 and 2002. They deployed a number of temporary instruments including one surface instrument for each event on site near the explosion. The last four explosions were conducted in a cavity approximately 4 meters high by 8 m wide by 30 m long (1000 $m^3$). The first three explosions were in two smaller chambers approximately 3 meters high by 4 meters wide with lengths of 17 meters (200 $m^3$) and 25 meters (300 $m^3$). Explosive yields ranged from 2500 kg to 10,000 kg, with charges consisting of TNT, ANFO and ammunition shells. The smallest explosion in the largest chamber appears to be fully decoupled, while the other explosions are partially coupled. A potentially important observation for monitoring is that even the fully decoupled 2500 kg explosion was detected at NORSAR, at a distance of about 150 km.

Near field data was recorded on pressure gauges in the chamber and adjacent tunnel, and on velocity gauges in boreholes at several locations near the chamber. We have completed data analysis of waveforms and spectra at the arrays, and both one-dimensional and three-dimensional numerical modeling of some of the near field data.

The results of the decoupling analysis are summarized in Figure 1.1 which shows observed decoupling factors for the Swedish chamber explosions together with predicted decoupling factors for a spherical cavity of the same volume. The decoupling factor contains an unknown scale factor, since we do not have data from a tamped explosion for comparison. The horizontal axis corresponds approximately to the overdrive factor above full decoupling. Both the data and the simulation show that the explosion remains nearly fully decoupled until the yield is increased by about an order of magnitude above the yield required for full decoupling. However, the decrease occurs at a lower yield for the observations than for the calculations, which is expected since the smallest dimension of the chamber is considerably closer to the explosion, and therefore is impacted by a stronger shock, than the wall of the equivalent volume spherical cavity.

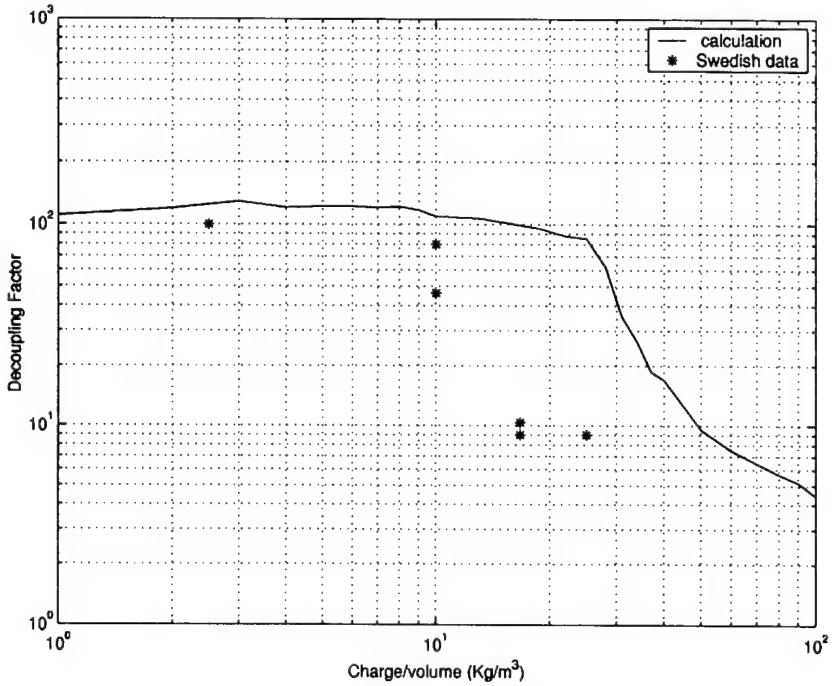


**Figure 1.1.** Observed and predicted decoupling factor for Swedish explosions. The Swedish explosions were in rectangular chambers in granite with volumes of 200 $m^3$, 300 $m^3$ and 1000 $m^3$. The calculations were for a chemical explosion in a 6.3 meter spherical cavity in granite (1000 $m^3$).

IDG has digitized a set of surface seismic data recorded from a series of Soviet high-explosive cavity decoupling tests conducted in a mine in Kirghizia in the summer of 1960. These decoupled tests were carried out in a variety of mined cavities in limestone with the objectives of assessing the dependence of cavity decoupling effectiveness on cavity volume, cavity shape, and charge emplacement geometry. In a previous study, Murphy et al (1997) conducted extensive analyses of free-field data recorded from these tests in the mine at distances on the order of 10-200 m. However, only limited waveform data were available from this regime, which made it difficult to determine the frequency dependence of the decoupling factors with a high degree of confidence. In the present study, seismic data recorded from a number of these tests on the surface at distances of 5 and 10 km from the source region have been recovered and digitized.

We have analyzed the digitized 3-component seismic data that was recorded at surface stations located 5 and 10 km away, and compared these results with those obtained earlier from close-in

data (Figure 1.2). High quality recordings are available from the 1 ton tamped and decoupled tests at the 5 km station, and the 6-ton tamped and decoupled tests at the 5 and 10 km stations. Results of detailed analyses of these data are consistent with those obtained from the previous analysis of the corresponding free-field data. In particular, all the decoupled tests conducted in the center of the cavities show low frequency chemical decoupling factors in the range 20-30, while that conducted 1 m from the wall of the 4.92 m radius cavity is about a factor of two smaller, indicating increased seismic coupling associated with nonlinear response of the cavity wall. The seismic signals observed from the 1 ton explosions conducted at the centers of the 2.88 m and 4.92 m radius cavities were found to be nearly identical, confirming that both of these tests were fully decoupled.

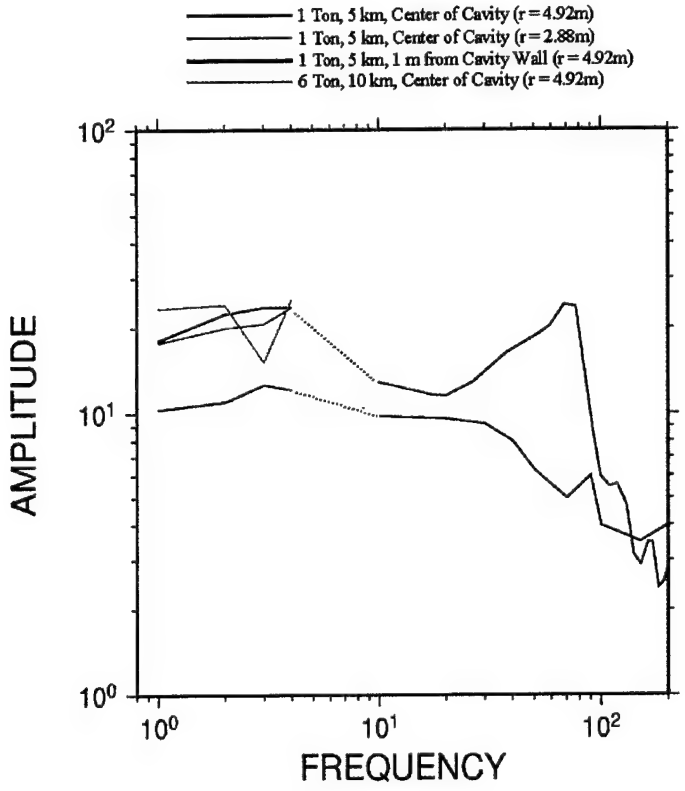


**Figure 1.2.** Frequency dependent decoupling factors for the 1 and 6 ton tests at the 5 and 10 km stations. Also shown are the corresponding results at higher frequency (i.e. 10 – 200 Hz) obtained previously by Murphy et al (1997) from the corresponding free-field data.

## 2. INTRODUCTION – DECOUPLING THEORY AND CRITERIA FOR FULL DECOUPLING

The source function for a fully decoupled explosion can be described as a pressure pulse applied to the wall of a cavity in an elastic medium. The actual physics is more complicated than this – there are reverberations in the cavity that cause high frequency spectral peaks, and the shock wave that hits the wall is stronger than an instantaneously applied pressure pulse corresponding to a uniformly pressurized cavity. However the simple model is useful for illustration and has many of the characteristics of a decoupled explosion. This simple description is also applicable to non-spherical cavities, however non-spherical cavities will become partially coupled at smaller yields because the smallest cavity dimension is closer to the source and will be impacted by a stronger shock wave than the spherical cavity.

The reduced velocity potential (RVP) for a pressure pulse $P(t)$ with derivative $\dot{P}(t)$ and corresponding Fourier transforms $P(\omega)$ and $\dot{P}(\omega)$ applied to the wall of a spherical cavity is (Stevens et al, 1991):

$$\dot{\psi}(\omega) = \dot{P}(\omega)\frac{R^3\omega_0^2}{4\mu}\frac{e^{i\omega/\omega_0}}{\omega_0^2 + i\omega\omega_0 - \left[(\lambda+2\mu)/4\mu\right]\omega^2} \tag{1}$$

where $\omega_0 = \alpha/R$, where $R$ is the cavity radius, $\alpha$ is the compressional velocity of the external medium and $\lambda$ and $\mu$ are the Lame constants of the external medium. For a step in pressure of magnitude $P_0$ applied at time $t=0$, $\dot{P}(\omega) = P_0$, and for this or any pressure pulse with static value $P_0$, in the low frequency limit, we have

$$\psi_\infty = P_0 R^3/4\mu \tag{2}$$

For an explosion in an air-filled cavity, the static value of the pressure is related to the yield $W$ by

$$P_0 = \frac{(\gamma-1)W}{V} \tag{3}$$

where $\gamma$ is the adiabatic expansion constant, which is approximately 1.2 for air and 1.3 for chemical explosion products, and $V$ is the cavity volume.

The "decoupling factor" $D$ is defined as the ratio of the fully coupled to decoupled source:

$$D = \psi_{tamped}/\psi_{decoupled} \tag{4}$$

The theoretical decoupling decreases with frequency. Figure 2.1 shows the coupled and decoupled source function and the frequency dependent decoupling factor obtained by taking the ratio of coupled to decoupled source. The decoupling factor decreases by an order of magnitude at high frequencies beginning at about 10 Hz.

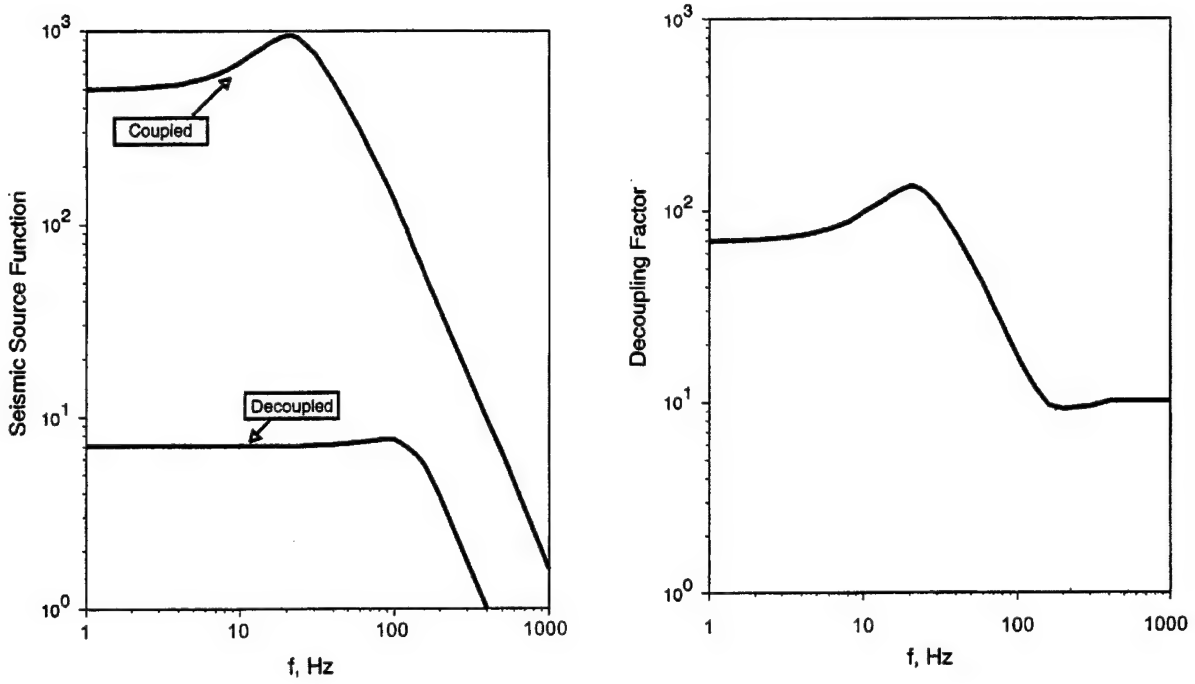


**Figure 2.1.** Source functions for fully coupled and fully decoupled 10 ton chemical explosions for a step pressure source in the cavity (left) and frequency dependent decoupling factor (right).

The criterion for full decoupling is usually expressed in terms of a requirement that the late-time, equilibrium pressure in the cavity be less than or equal to some constant, k, times the overburden pressure (Herbst et al, 1961):

$$\frac{(\gamma-1)W}{V} \leq k\rho gh \tag{5}$$

where $k$ is between 0.5 (Latter) and 1.0 (Patterson), and $\rho gh$ is the overburden pressure at depth $h$. The Swedish chamber explosions discussed in section 3 of this report are at 100 meters depth in granite. Figure 2.2 shows the Latter criterion for full decoupling together with the actual parameters calculated from the known depth and volume for each of these explosions. All of the explosions exceed the Latter threshold, although one explosion (2500 ton in 1000 $m^3$ chamber) is close to fully decoupled.

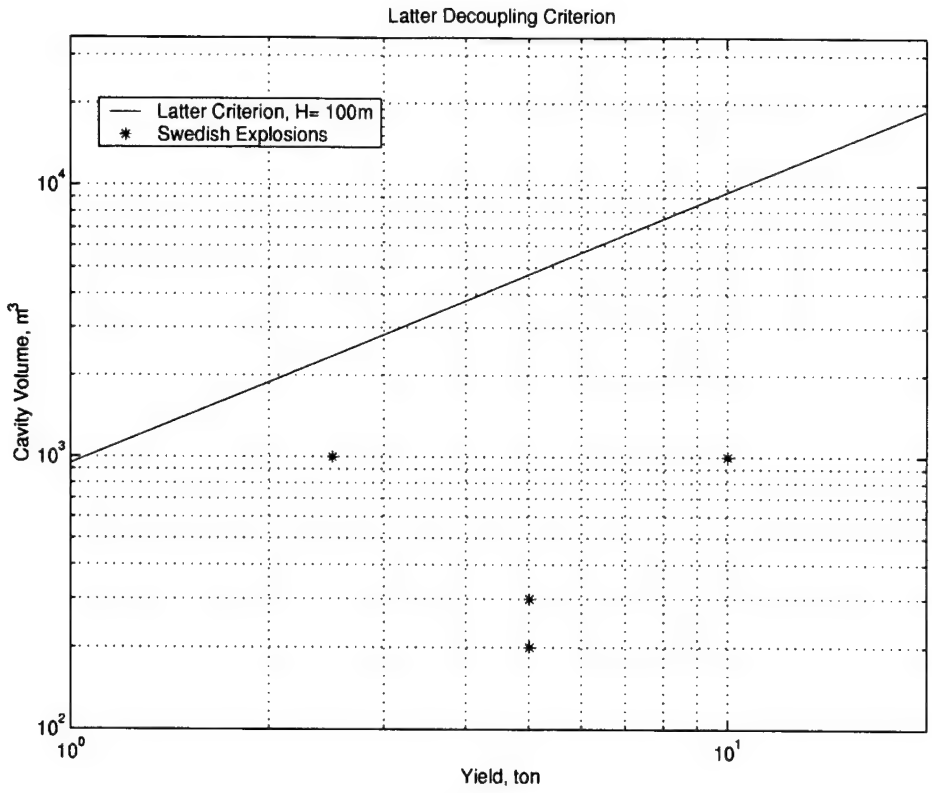


**Figure 2.2.** Latter decoupling criterion calculated for the conditions of the Swedish chamber explosions. The actual values for the Swedish chamber explosions are marked.

# 3. DECOUPLED EXPLOSIONS AT ÄLVDALEN, SWEDEN

At a site within Älvdalen Skjutfält in central Sweden, a number of decoupled chemical explosions have been carried out within underground cavities at a depth of approximately 100 meters. At Mossibränden, a site less than 20 kilometers from this chamber, outdated ammunition is routinely detonated at ground level by the Swedish Armed Forces. The seismic signals from both categories of explosions have been collected into a database and analyzed. The sites are in very close proximity to each other and are approximately equidistant from the seismic arrays HFS (Hagfors, Sweden), NRS (NORES, Norway), and the wide aperture NORSAR array (Figure 3.1). The surface explosions at Mossibränden were described and analyzed in our previous annual report (Stevens et al, 2002) and will not be repeated here. Following is a summary of the decoupled explosions and data.

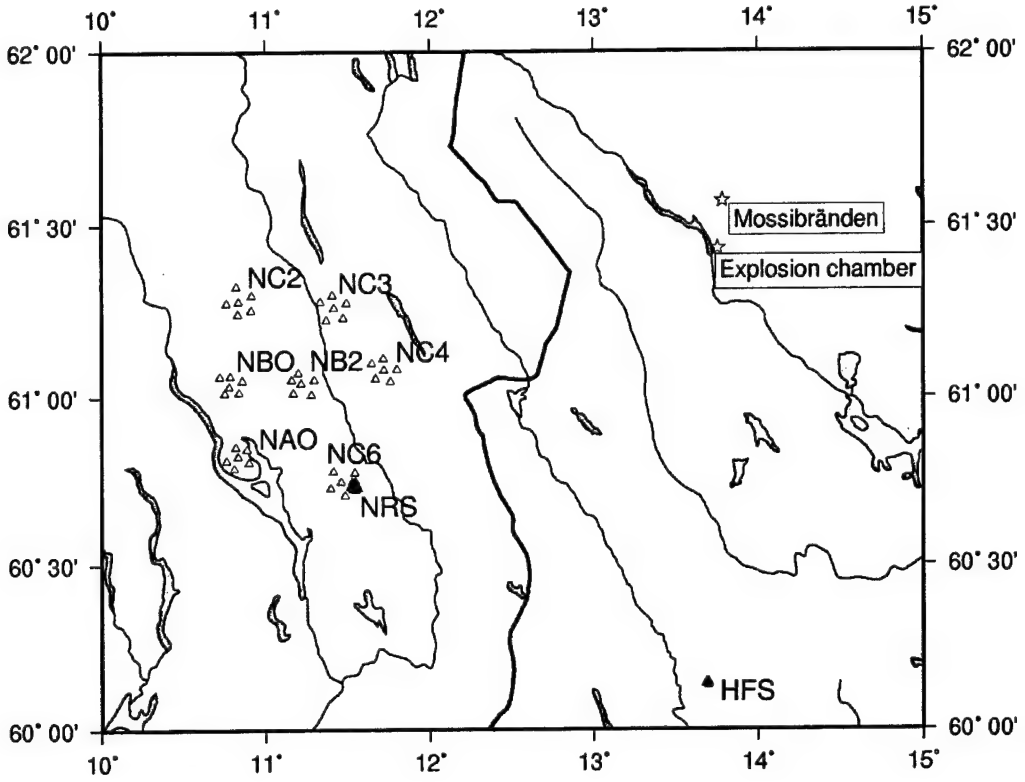


**Figure 3.1.** The location of the explosion sites relative to the HFS and NRS arrays and the NORSAR (NOA) sub-arrays. The solid red line is the Norway/Sweden national boundary.

## 3.1 Decoupled Chamber Explosions

Figure 3.2 shows the location of the large chamber, the adjacent tunnel complex, and the location of pressure sensors and accelerometers that recorded data from the explosions. The entrance to the chamber is open, so the blast wave from the chamber explosion propagates out of the chamber and down the tunnel.

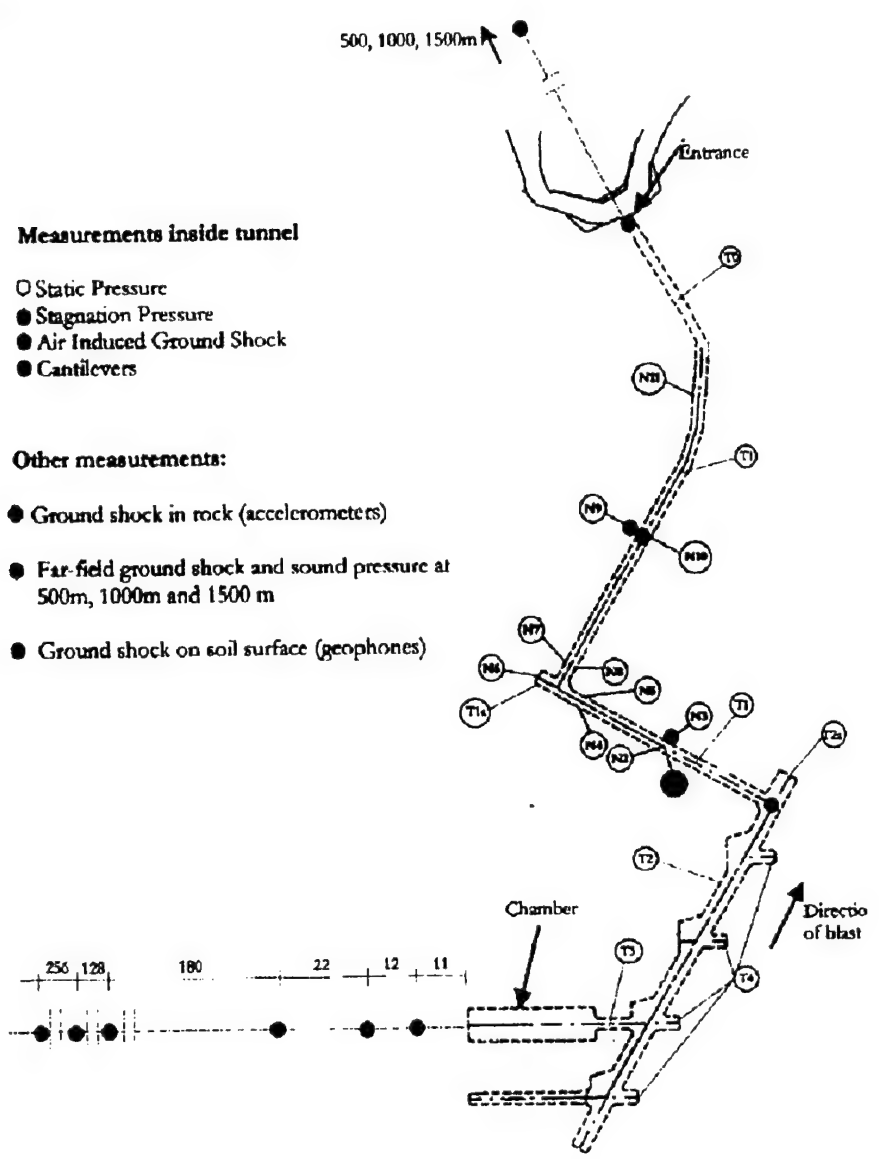


**Figure 3.2.** Location of the chamber in relation to the entrance and the pressure sensors in the access tunnels.

Figure 3.3 shows the location of the underground chamber relative to the surface and local instrumentation. The set of events from the underground cavities includes 3 different quantities of explosives in nearly co-located chambers of 3 different sizes. The cavity explosions, which comprise two separate series of experiments (1987-89 and 2000-2002) are listed in Table 3.1. All chambers are open to the same tunnel system. The 2000-2002 series of explosions were conducted in a cavity approximately 4 meters high by 8 m wide by 30 m long (1000 $m^3$). The 1987-1989 explosions were in two smaller chambers approximately 3 meters high by 4 meters wide with lengths of 17 meters (200 $m^3$) and 25 meters (300 $m^3$).

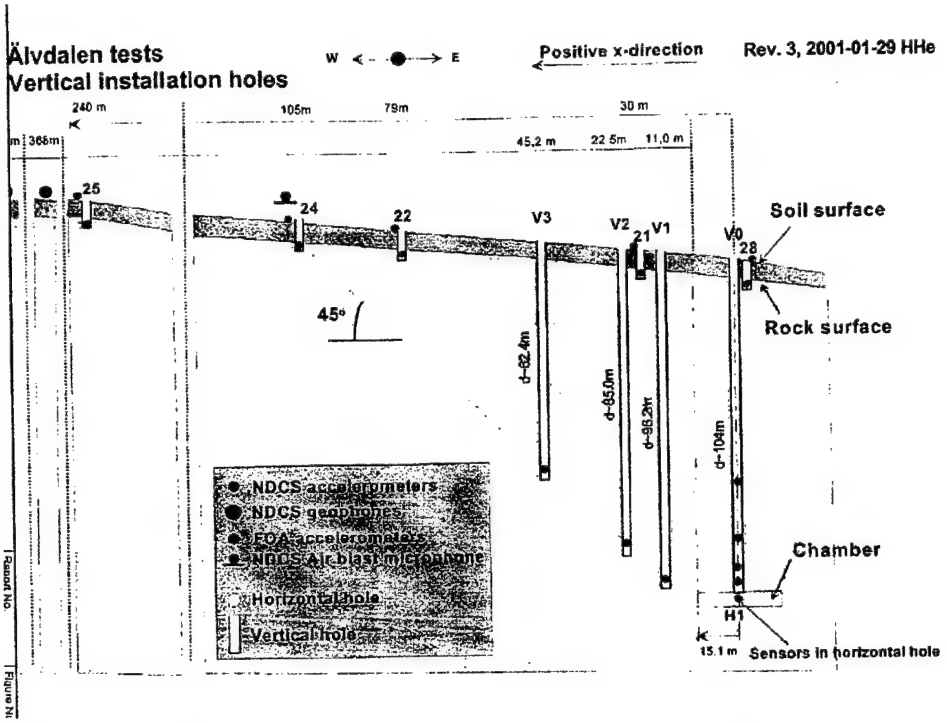


**Figure 3.3.** Location of chamber relative to the surface and local instrumentation.

**Table 3.1.** Cavity decoupled explosions at the Älvdalen site. Origin times of the 1987-89 events were estimated from arrival times at NORES. Origin times of the 2000-2001 events were determined from a station at the explosion site.

| Origin ID | Explosion origin time | Explosion charge (kg) | Explosive | Chamber Volume ($m^3$)[a] | Charge/Volume ($kg/m^3$) |
|---|---|---|---|---|---|
| 1987C146 | 1987-146:10.47.38.2 | 5000 | ANFO[b] | 300 | 16.7 |
| 1987C259 | 1987-259:10.36.13.0 | 5000 | ANFO | 200 | 25.0 |
| 1989C263 | 1989-263:10.06.03.5 | 5000 | ANFO | 300 | 16.7 |
| 2000C348 | 2000-348:10.03.02.0 | 10000 | TNT | 1000 | 10 |
| 2001C150 | 2001-150:10.03.56.2 | 2500 | TNT | 1000 | 2.5 |
| 2001C186 | 2001-186:10.41.23.5 | 10000 | Ammunition Shells | 1000 | 10 |
| 2002C164 | 2002-164:08.59.25.1 | 10000 | TNT/powder | 1000 | 10 |

[a]Chamber volume excludes access tunnel.
[b]The ANFO explosive used in the 1987 and 1989 events had an explosion equivalent of 0.82 of TNT.

## 3.2 Regional Data for Decoupled Chamber Explosions

Figure 3.4 shows unfiltered waveforms for the first 6 underground explosions in Älvdalen. The signals resulting from the three events from 1987 and 1989 (a, b and c) have much larger amplitudes than the later events (d, e and f) which probably reflects the differences in charge/cavity volume as displayed in Table 3.1. Despite the larger amounts of explosives used, the larger chamber size results in far weaker signals. The signal from event 2001C150 (2500kg TNT in the $1000m^3$ chamber, plot e) is indistinguishable from the noise without filtering of the data.

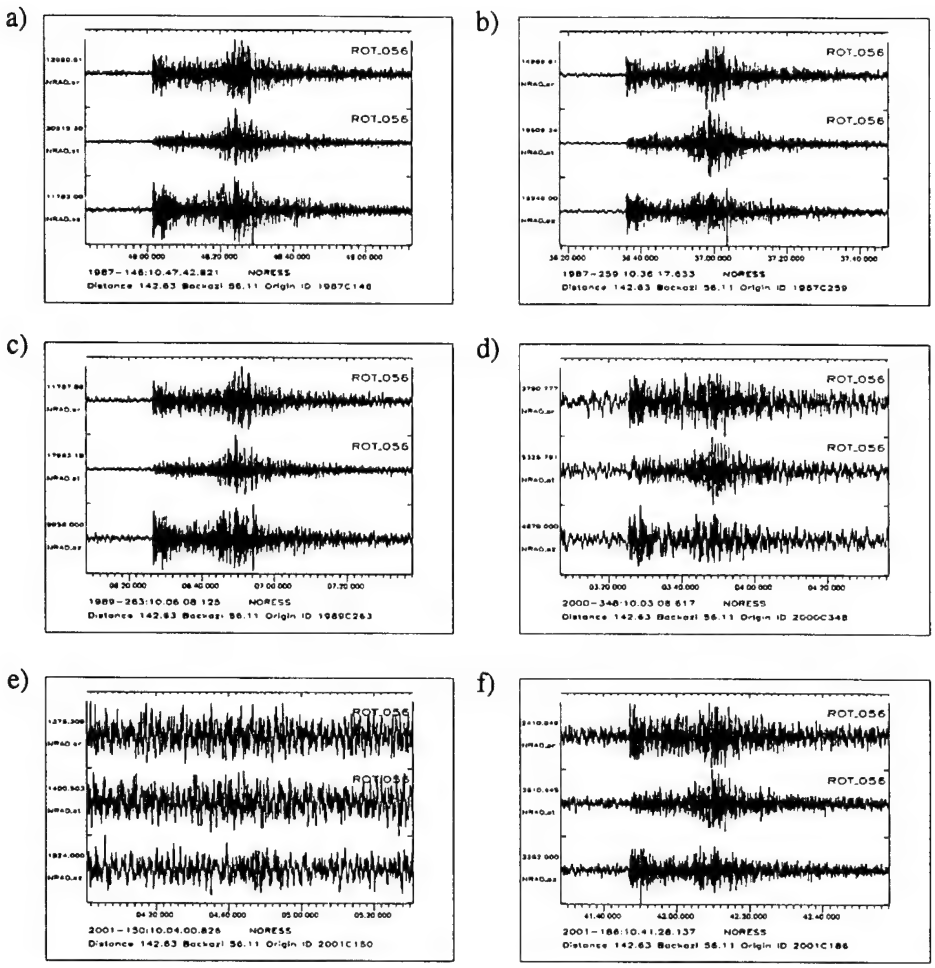


**Figure 3.4.** Unfiltered waveforms for the 6 decoupled explosions from the 3-component NRA0 instrument of the NORES array. Waveforms are rotated into radial and transverse components. Origin ID codes are as given on the diagrams. Explosives and chamber sizes are a) 5000kg ANFO, 300m3 chamber, b) 5000kg ANFO, 200m3 chamber, c) 5000kg ANFO, 300m3 chamber, d) 10000kg TNT, 1000m3 chamber, e) 2500kg TNT, 1000m3 chamber, and f) 10000kg ammunition shells, 1000m3 chamber.

In order to quantify the differences between these six events, we examine the power spectral density. For each component, three time windows were defined corresponding to the P arrival, S arrival, and pre-event noise (Figure 35). A 5 second window of waveform data was extracted immediately after the P onset, and a 10 second window immediately after the S onset. A 10 second window ending 2 seconds before the P onset was defined in order to quantify the level of noise which is expected in the signal. Power spectral density was calculated for each time window. In order to provide a common basis for comparison, we have converted all spectra to the characteristics of the HFS response. Unlike the NORES response, the HFS response is flat to velocity over the passband. Converted power spectral density, averaged over the vertical components of the NORES array are shown in Figure 6 for all 6 explosions listed in Table 3.1, for frequencies up to the Nyquist frequency of 20 Hz.

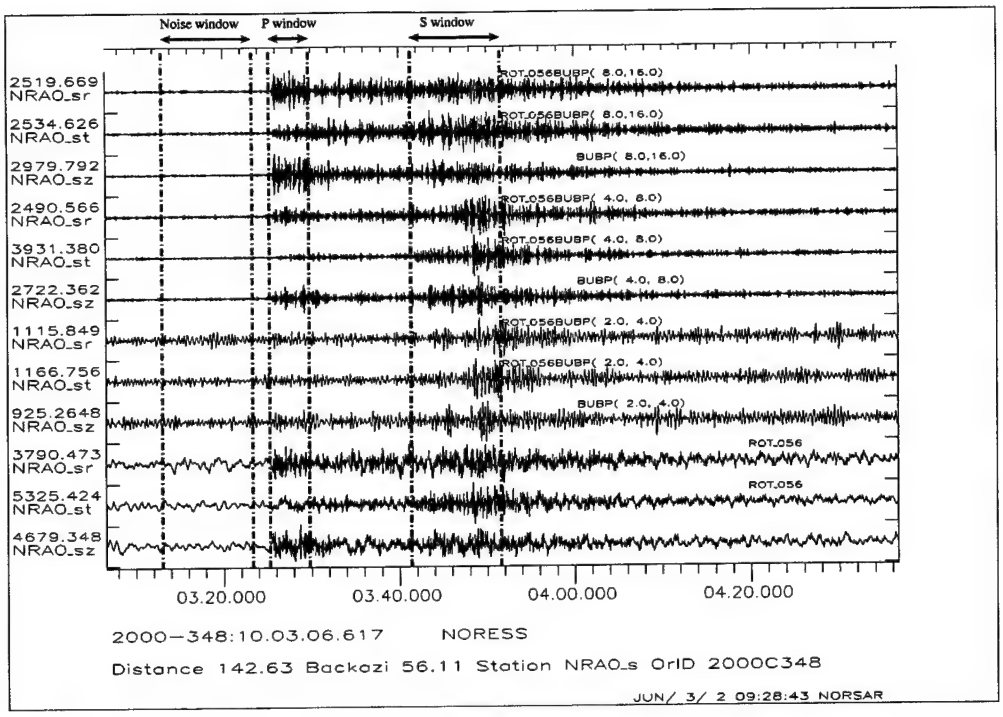


**Figure 3.5.** Waveform data for event 2000C348 as recorded by the NRA0 instrument. The twelve traces shown are displayed in groups of three. The lowermost 3 traces are unfiltered data and the remaining traces are filtered with a Butterworth band-pass filter in the frequency bands 2.0 - 4.0 Hz, 4.0 - 8.0 Hz and 8.0 - 16.0 Hz as indicated. Each group of three traces contains the vertical component (z) and the rotated radial (r) and transverse (t) traces. Also indicated are the time windows used to calculate power spectral density.

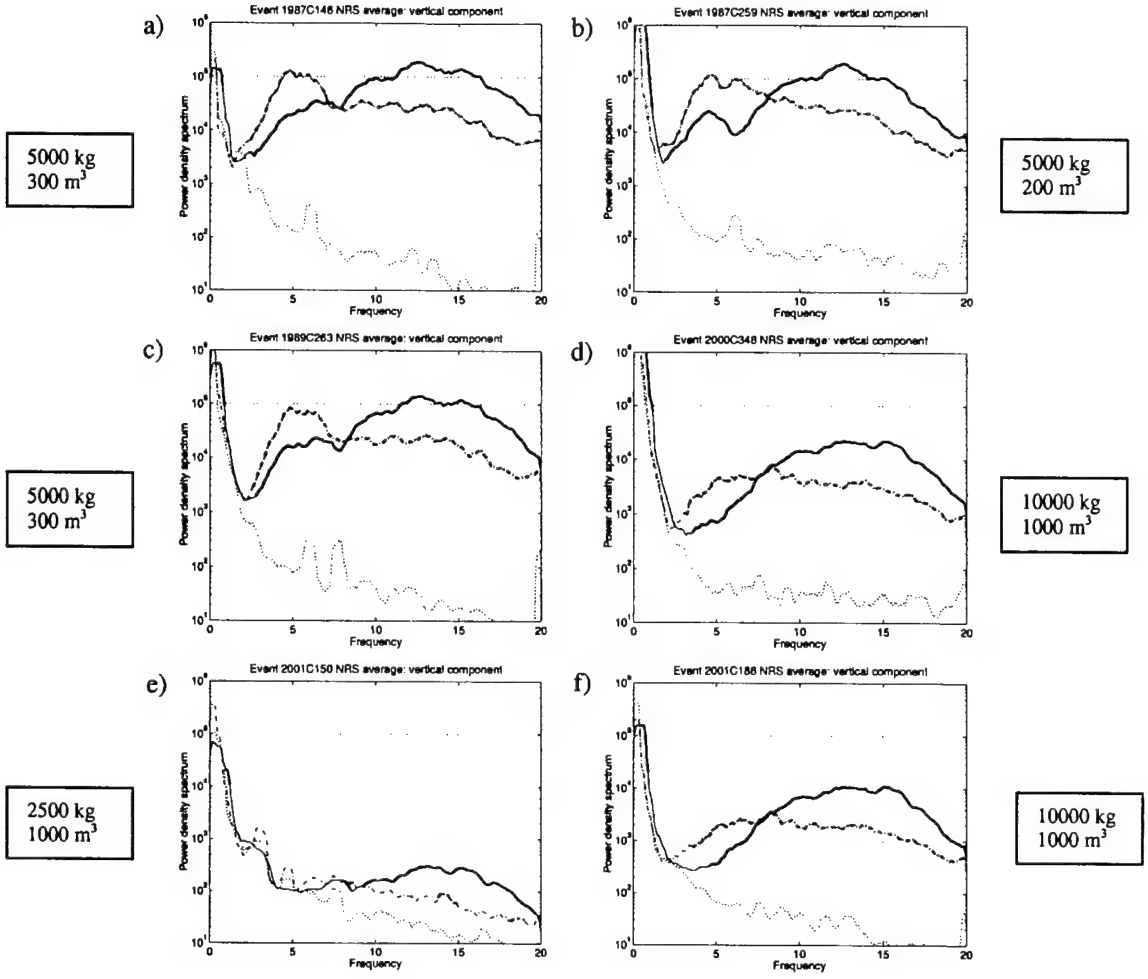


**Figure 3.6.** Average power spectral density (PSD) from NORES vertical component data for the six decoupled explosions as indicated; all spectra are converted to HFS response. The solid red line indicates PSD for the P window, the dashed blue line indicates PSD for the S window and the dotted black line indicates PSD for the noise window. At frequencies where the PSD for the P or S window is less than 4.0 times that for the noise window, the signal spectrum is shown as a thin line.

The results shown in Figure 3.6 clearly show the effect of substantially greater decoupling for the larger chamber relative to the smaller chamber. In the dominant frequency band of the spectra, the measured decoupling is about a factor of 5-10, and it becomes larger at lower frequencies, in agreement with theory.

Using the average of the vertical component traces from the NRS, NOA and HFS arrays in the P arrival time window, we compare the power spectral density of all seven cavity explosions listed in Table 3.1. The result is shown in Figure 3.7.

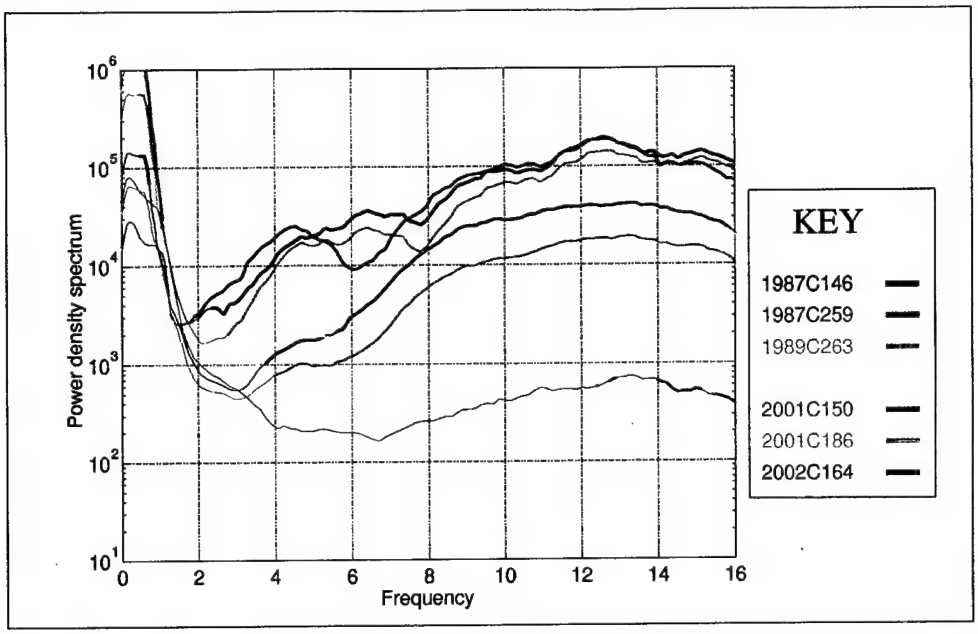


**Figure 3.7.** Power spectral density for the P time window averaged over all vertical component instruments for the arrays NOA, NRS and HFS. Thin lines indicate that the ratio PSD(signal)/PSD(noise) was below 4.0 for a given frequency. Events 1987C146, 1987C259 and 1989C263 only include instruments from the NORES array. Event 2002C164 only includes instruments from the HFS and NOA arrays.

## 3.3 Near Field Recordings (Accelerograms and Pressure Recordings) From the Decoupled Explosions

Near-field accelerometer recordings have been made available by Forsvarsbygg (contact person: Geir Arne Grønsten) for the decoupled explosions in 2000 and 2001 (2000C348, 2001C150 and 2001C186 in Table 3.1), with additional pressure measurements from within the detonation chamber for the two decoupled explosions in 2001.

### 3.3.1 Accelerograms

The acceleration data consists of three-component recordings in vertical boreholes and two two-component (vertical + parallel to long axis of chamber) at soil and rock sites. The boreholes are located at distances of 11, 22.6 and 45.2 m west of the chamber wall, while the surface accelerometers have an assumed location 96.5 m west (assumed along the same line) of the chamber wall. The accelerometer locations relative to the detonation chamber are shown in Figure 3.8.

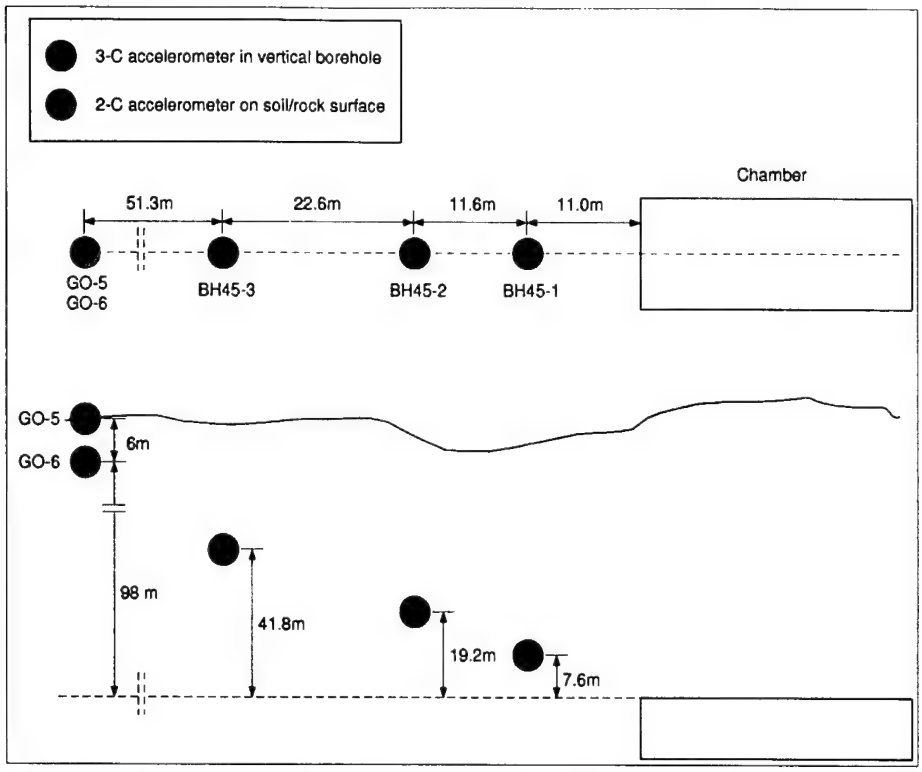


**Figure 3.8.** Accelerometer configuration relative to detonation chamber. Note that BH45-1,2,3 correspond to locations V1, V2 and V3 in figure 3.3.

Raw data for each of the three explosions is shown in Figures 3.9-3.11, and filtered comparisons of the three explosions at the same station are shown in Figures 3.12-3.15.

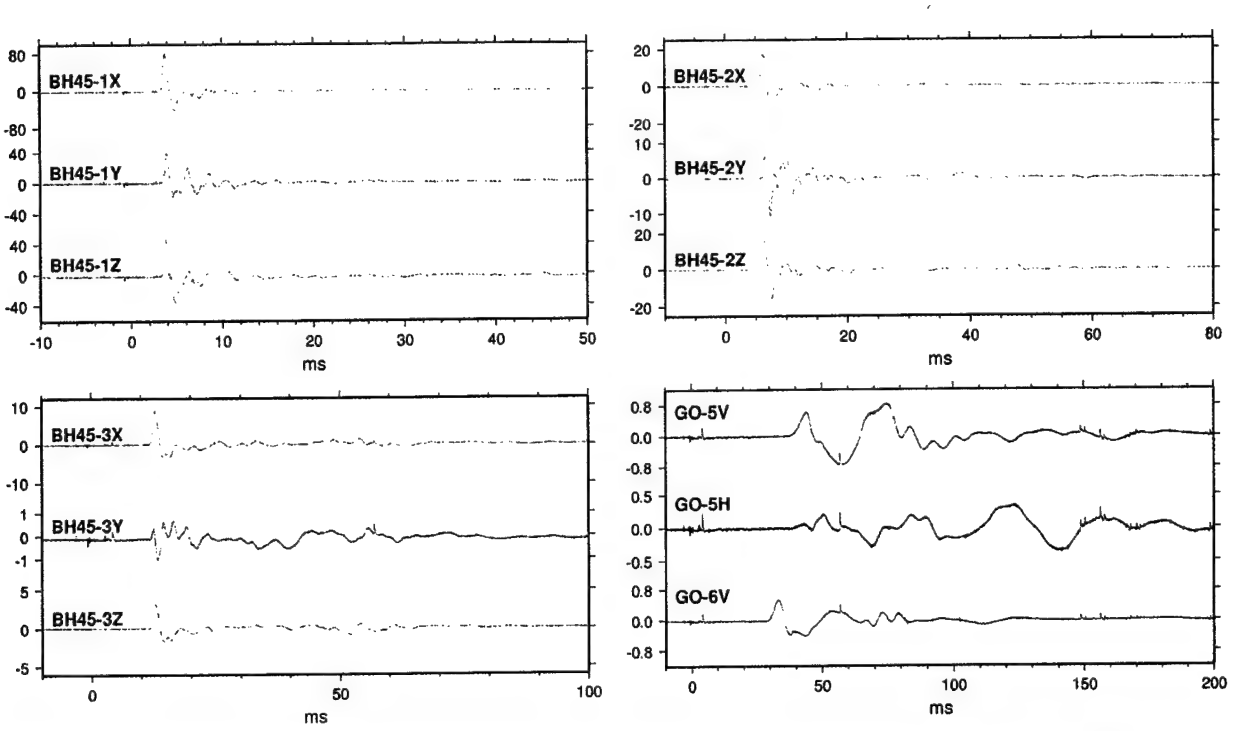


**Figure 3.9.** Near-field accelerometer recordings of the 10,000 kg TNT explosion on December 13, 2000 (2000C348). Vertical scale is in g.

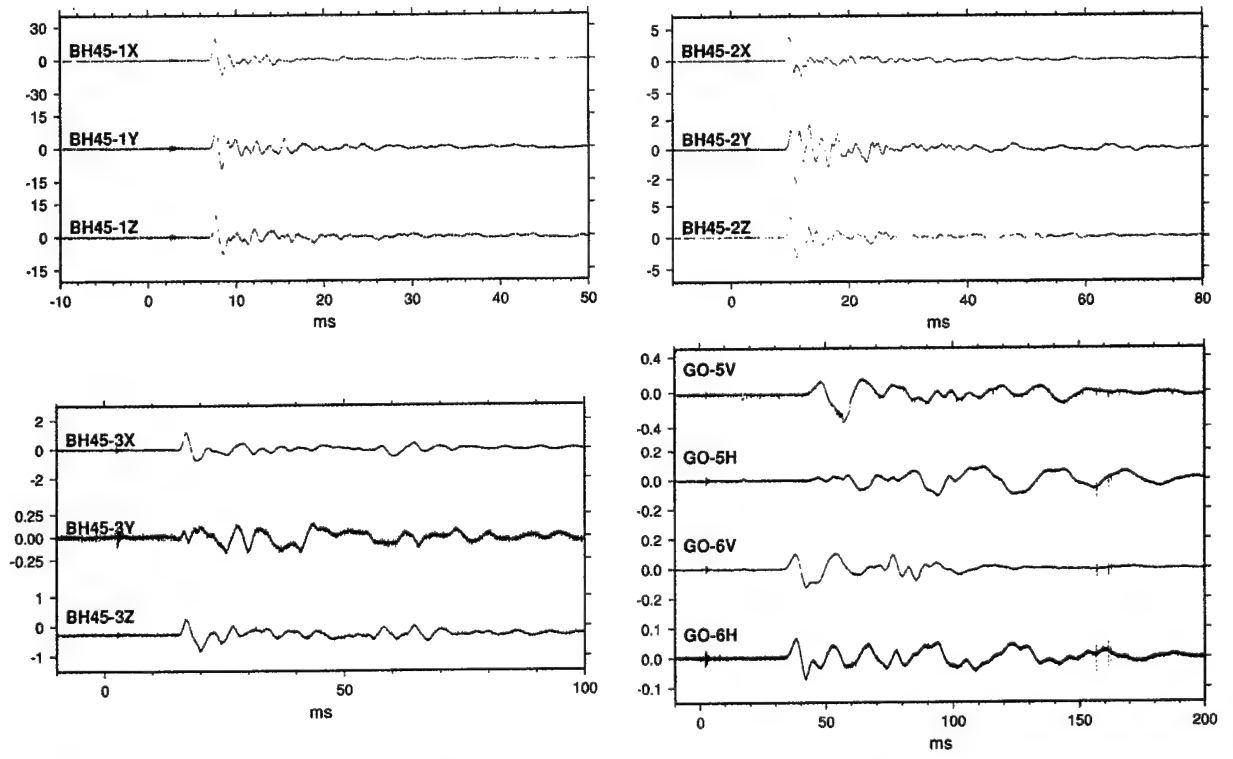


**Figure 3.10.** Near –field accelerometer recordings of the 2,500 kg TNT explosion on May 30, 2001 (2001C150). Vertical scale is in g.

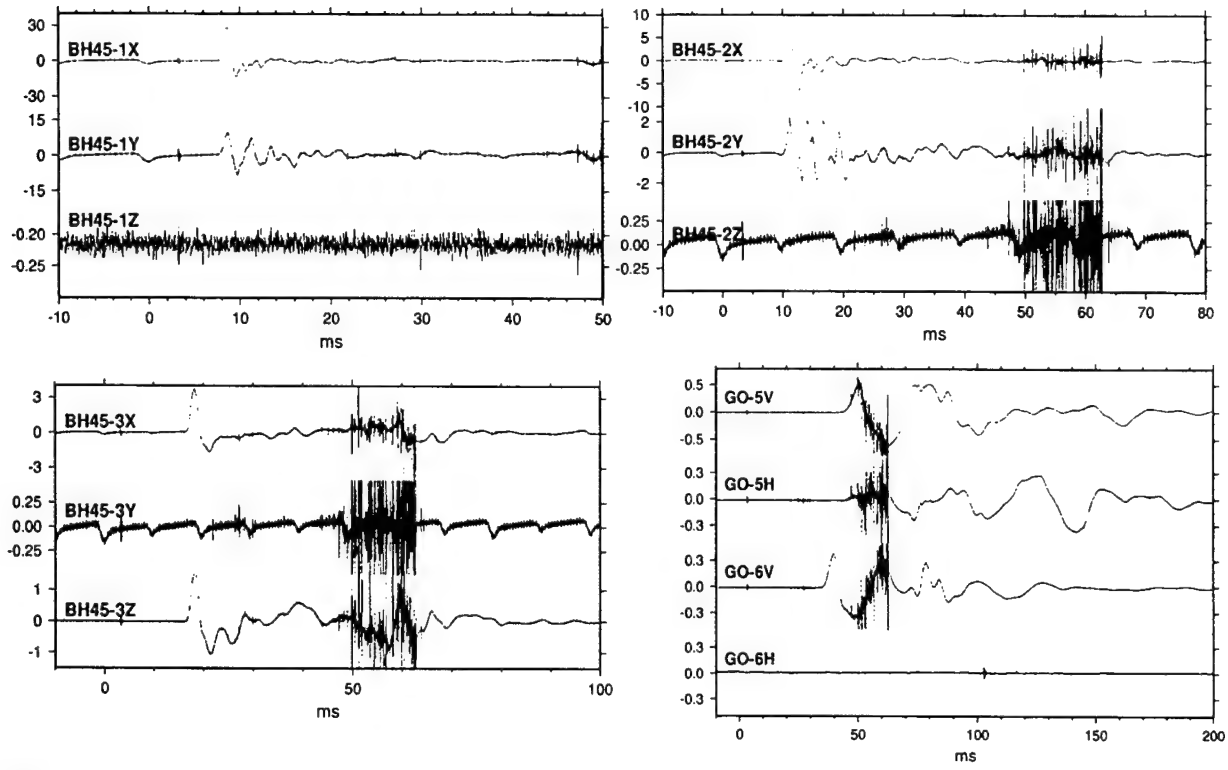


**Figure 3.11.** Near-field accelerometer recordings of the 10,000 kg ammunition shell explosion on July 5, 2001 (2001C186). Vertical scale is in g. Note the significantly lower accelerations compared to the 10,000 kg TNT explosion on December 13, 2000 in Figure 3.9.

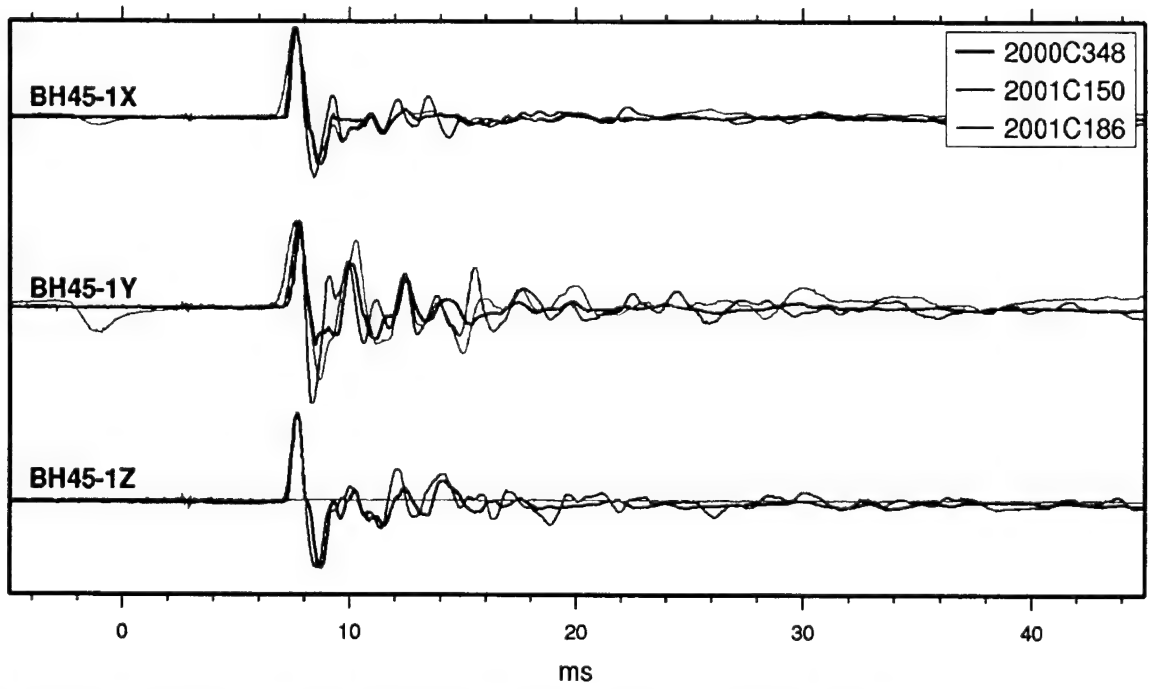


**Figure 3.12.** Comparison of the three explosions recorded at the closest borehole (BH45-1). The individual traces have been lowpass filtered, and are scaled by peak value and roughly aligned on the first arrival. Note that the vertical (Z) channel for 2001C186 is defective.

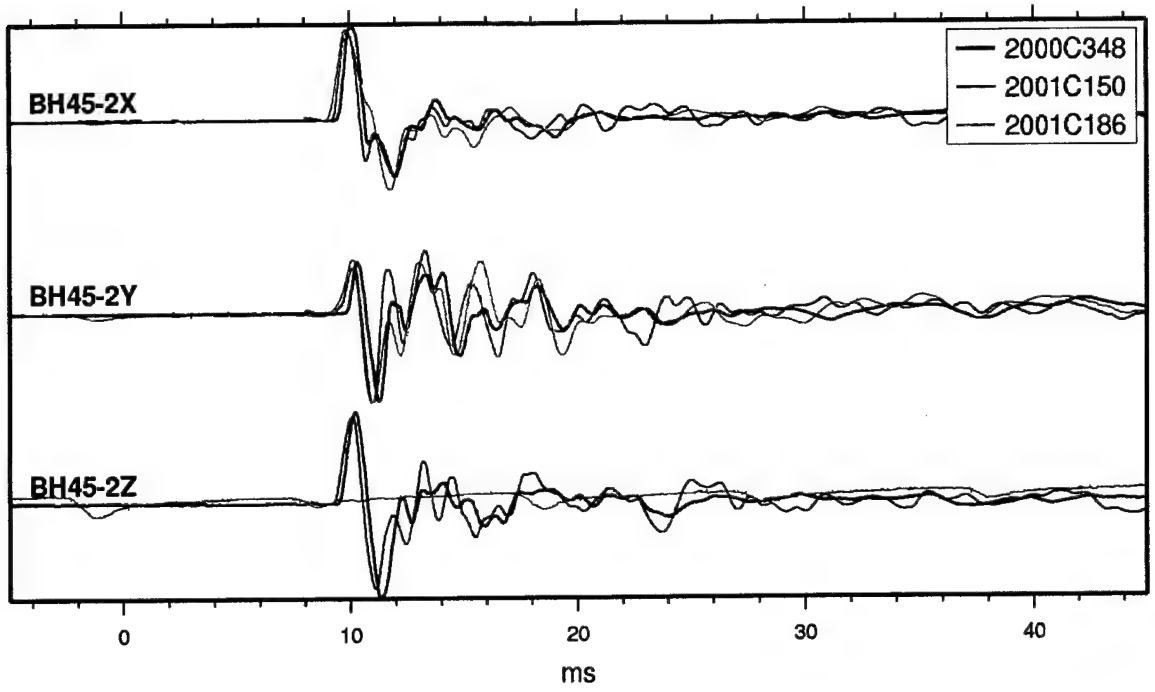


**Figure 3.13.** As Figure 3.12, but for the borehole located 23 m west of the chamber edge (BH45-2). The vertical (Z) channel for 2001C186 is defective also here.

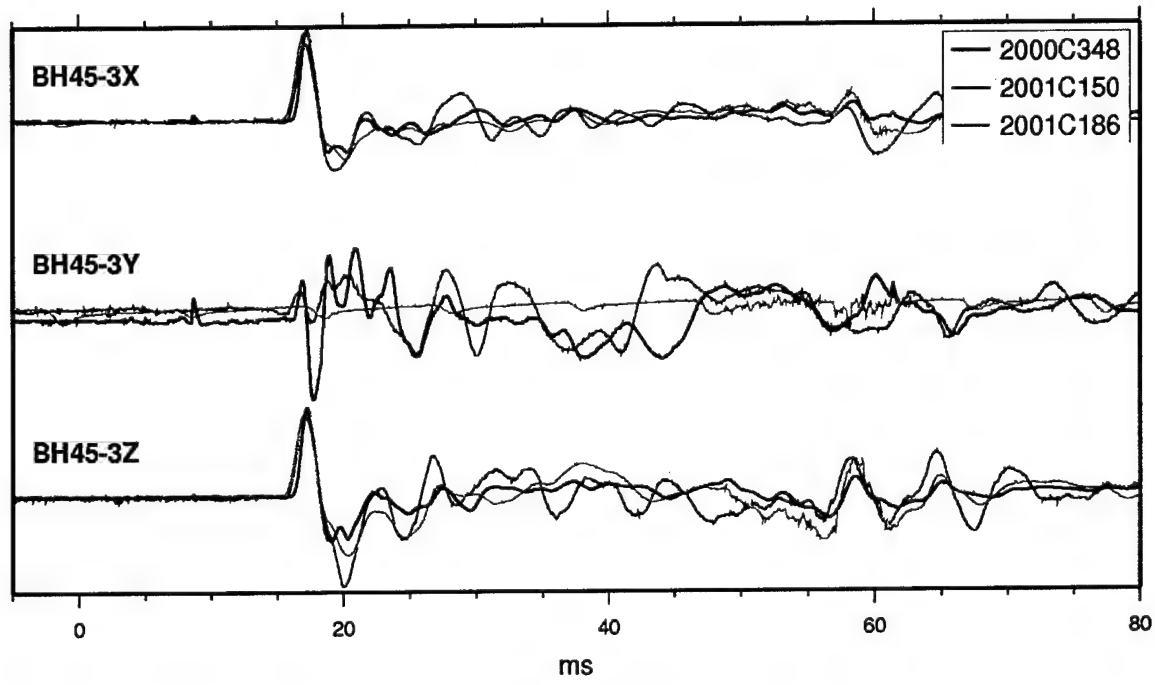


**Figure 3.14.** As Figures 3.14 and 3.15, but for the borehole located 45 m west of chamber wall (BH45-3). The transverse (Y) channel is defective for the 2001C186 explosion.

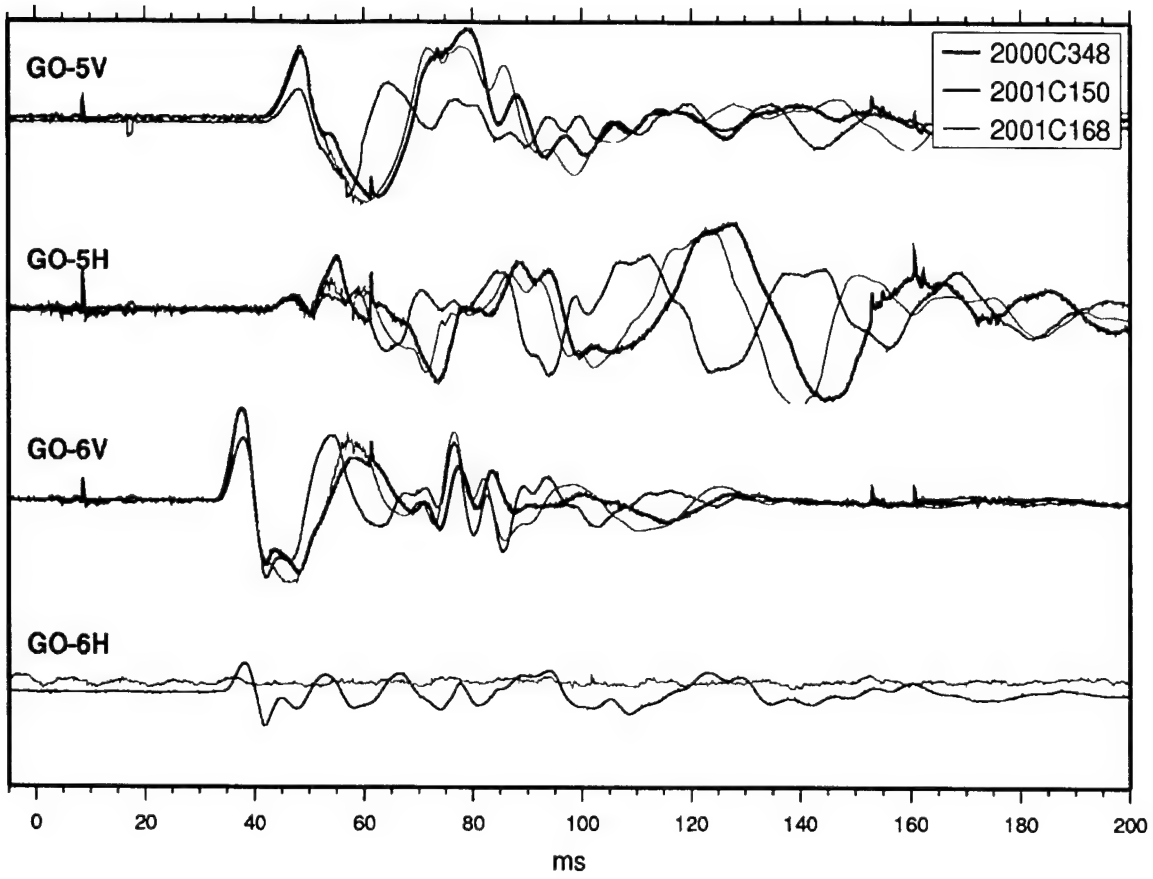


**Figure 3.15.** As Figures 3.12-3.14, but for instruments located at the soil surface (GO-5) and soil-rock interface (GO-6). The GO-6H (soil-rock interface, horizontal) channel is unavailable for 2000C348 and defective for 2001C186.

## 3.4 Numerical Simulations of Near Field Data From Swedish Decoupled Chamber Explosions

We are attempting to simulate shock wave propagation from three explosive tests that were conducted in the large Älvdalen chamber in hard rock. The tests are identified as Test 3, Test 4a and Test 4b (Gronsten, Gronsten et al.), and correspond to decoupled explosions 2000C348, 2001C150, and 2001C186, respectively. The chamber volume was approximately 1000 cubic meters. Test 3 used 10,000 kilograms (10 tons) of TNT, while Test 4a used 2.5 tons of TNT. For each of these tests, the TNT mass was divided into 10 equal masses that were emplaced well above the chamber floor on styrofoam. The axisymmetric explosive emplacement (about the long axis of the chamber) was in two rows of 5 TNT masses each, with row separation of 5 meters and 6 meters between the center of each of the charge masses in a row. Test 4b had 10 tons TNT equivalent, consisting of 1450 155-mm shells emplaced similarly to the earlier tests in 10 clusters of 145 shells each.

Three-dimensional accelerometers, placed in vertical holes drilled from the surface, were used to record the near field motions from the explosions. We generated particle velocity records by time-integrating these accelerometer records. In the following sections we describe two sets of

calculations: spherically symmetric finite difference calculations for an equivalent volume sphere in granite, and 3D finite difference calculations in which we model the known cavity geometry and layout of explosive in the chamber. In these calculations we model the chamber as sealed at the time of each explosion so that all explosive materials stay in the chamber. However, air pressure measurements at various places in the tunnel complex confirm that, in fact, the chamber was not sealed. Future work will investigate the effect of the pressure reduction caused by the chamber opening to the tunnel.

### 3.4.1 Test Geometry

Test chamber dimensions are roughly 8 meters in width, 3.68 meters in height, and 34 meters in length. The long axis of this chamber, the parallel direction in the original data reports (our x axis), is in the E-W direction, i.e., in the plane of the three grouted, vertical drill holes containing the accelerometers. This vertical x-z plane (the z axis points upward) is presumed to intersect the center of the chamber, providing a theoretical plane of symmetry since the TNT was emplaced symmetrically about the long axis of the chamber. Thus, the predominant motions at the gauge locations should be in the positive x and z directions, with little motion expected in the horizontal N-S (our y) direction.

The three accelerometer packages are located along a line in this vertical plane of symmetry at an angle of 45 degrees to the vertical. This line does not go through the center of the chamber. Thus, the (spherical) radial direction for our 1D calculations is not along the axis of the three accelerometers. These three gauges, designated as V1, V2, and V3, are at slant ranges (radial distances) of 27.7, 43.1, and 74.4 meters respectively from the center of the chamber. The coordinates of these gauges relative to the center of the chamber (xc and zc) and relative to the closest edge, the top for the z coordinate (xe and ze), are given in Table 3.2.

**Table 3.2.** Coordinates of gauges V1, V2, and V3 relative to center (xc, zc) and closest edge (xe, ze) of the explosion chamber for Tests 3, 4a, and 4b.

| Gauge # | Slant range from center (m) | xc (m) | zc (m) | xe (m) | ze (m) |
|---|---|---|---|---|---|
| V1 | 27.7 | 26.1 | 9.3 | 11.0 | 7.6 |
| V2 | 43.1 | 37.7 | 20.9 | 22.6 | 19.2 |
| V3 | 74.4 | 60.3 | 43.5 | 45.2 | 41.8 |

### 3.4.2 Data Analysis

The accelerometer measurements (and integrated particle velocities) are obtained in the x, y, z, coordinate system defined above. From the raw data figures, we have compiled a table of results for the first signal at each gauge location. For many of the results in Table 3.3, comparisons between the three explosions appear to be at least qualitatively in line with expectations. Lower peak velocities at the gauges for Test 4a compared with Test 3 are consistent with the more decoupled explosion. The lower peaks for Test 4b, for the same mass of explosive as Test 3, could be due to a lower energy content than expected in the ammunition or a slower detonation compared with the pure TNT detonated in Test 3. Test 4b does give higher peaks than the more decoupled Test 4a.

**Table 3.3.** Values of arrival time, time of first peak velocity, rise time, and peak particle velocity components for Tests 3, 4a, and 4b in 1000 $m^3$ chamber. Times for y component are shown in parentheses if different from other components.

| Test # Gauge # | Arrival time of first signal (ms) | Time of first peak (ms) | Rise time to peak (ms) | Peak of x component (cm/s) | Peak of z component (cm/s) | Peak of y component (cm/s) |
|---|---|---|---|---|---|---|
| **Test 3** | | | | | | |
| **10 tons TNT** | | | | | | |
| V1 | 3.4 | 4.1(4.3) | 0.7 | 41.5 | 22 | 16.4 |
| V2 | 5.7(6.0) | 6.8 | 1.1 | 12 | 10.8 | 3.1 |
| V3 | 12 | 13.8 | 1.8 | 9.4 | 3.5 | -0.64 |
| **Test 4a** | | | | | | |
| **2.5 tons TNT** | | | | | | |
| V1 | 7.2 | 8.0 | 0.8 | 10 | 4.8 | 4.2 |
| V2 | 9.5 | 10.4 | 0.9 | 2.7 | 2.2 | 0.7 |
| V3 | 16.1 | 18.1 | 2.0 | 1.5 | 0.4 | 0 |
| **Test 4b** | | | | | | |
| **10 tons Ammo** | | | | | | |
| V1 | 7.9 | 9.2 | 1.3 | 21.5 | defective | 7.2 |
| V2 | 10.1 | 12.1 | 2.0 | 8.1 | defective | 1.5 |
| V3 | 16.9 | 19.4 | 2.5 | 5.7 | 2.3 | defective |

Note that the y component of the peak particle velocity, expected to be negligible because of the plane of symmetry of the experiment, is a significant fraction of the x and z velocity components, particularly at gauges V1 and V2. This could indicate that the individual drill holes from the surface were not aligned correctly. The y velocity components from Test 3 are less likely to be the result of asymmetric explosive detonation, since the direction of this y motion has changed between gauges. For Test 4b, the vertical channels at V1, V2, and the transverse channel at V3, all became defective for this July, 2001 explosion. Therefore, these defective records are all excluded in the following discussions.

The later arrival times in Tests 4a and 4b compared to Test 3 must be investigated further with our calculations. We would expect some small delay for the smaller event since the propagation speed of the signal through the air is nonlinear with amplitude. The spherically symmetric calculations will tell us the magnitude of the time delay for the explosive centered in a spherical cavity. More detailed multi-dimensional calculations may be needed for the actual test configurations.

The arrivals for the 10-ton ammunition Test 4b are roughly the same as for the smaller event. One question to be asked is whether the first test damaged the surrounding rock, thus reducing the wave speed. The measured rise times of Test 4a, statistically the same as for Test 3, imply that the rock has not been damaged significantly. The larger rise times for Test 4b may be due to a more diffusive ammunition detonation. The later arrivals for this test may also be linked to the use of ammunition rather than pure TNT.

Table 3.4 shows the apparent P-wave velocities calculated between individual gauges from the arrival time information and the distance between gauges. These apparent wave speeds do not show any statistically significant decreases due to the earlier shots, particularly near the chamber, where the most damage to the rock would be expected. The large apparent wave speeds in the first (relatively short) segment may be an aberration, since the chamber is clearly neither a point source nor a spherical source and the most direct ray from the center of the long, explosive-filled chamber to gauge V2 does not lie along the ray from the chamber to gauge V1.

**Table 3.4.** Apparent P-wave velocities calculated between individual gauges for Tests 3, 4a, and 4b.

| **Test #** | | **3** | **4a** | **4b** |
|---|---|---|---|---|
| Segment | Segment length (m) | P-wave speed (m/s) | P-wave speed (m/s) | P-wave speed (m/s) |
| V1-V2 | 16.41 | 7133 | 7132 | 7457 |
| V2-V3 | 31.96 | 5073 | 4842 | 4700 |
| V1-V3 | 48.37 | 5624 | 5641 | 5374 |

The discussions so far have dealt with the first signals only. Some description of the differences between test results for the longer term signals follows. For Test 3, a slow rise in particle velocity is measured at gauge V1, beginning about 30 ms and peaking at about 200 ms with a magnitude of 30 cm/s, about 75% of the first peak. This second signal is not seen at the two other gauges for Test 3. For Test 4a, a similar second signal begins at gauge V1 at 130 ms, peaks at 270 ms with a magnitude of 17 cm/s, much larger than the first peak. Again this signal is not seen on the other two gauges. Thus, this signal is unlikely to be due to any interaction with the free surface, located approximately 100 meters above the chamber. For Test 4b, a large second signal is seen on all three gauges, with a magnitude of 12 cm/s at V1, 9 cm/s at V2, and 6 cm/s at V3. Detailed two-dimensional calculations will be needed to understand these later time measurements.

For comparison with spherically symmetric one-dimensional calculations to be discussed below (we ignore the free surface effect), we rotated the measured values of the x and z components of the particle velocities about the line from the center of the test chamber to the gauge to obtain the radial and tangential (in-plane) components, i.e., to cylindrical, rather than spherical, components. The recorded y components of the acceleration (and particle velocities) were thus treated here as a measure of unexpected large asymmetries in the results of a theoretically axisymmetric experiment.

These asymmetric accelerometer measurements are not yet understood. Possible explanations include inhomogeneities in the surrounding rock, the precision of the axisymmetric gauge emplacements, and/or the symmetry of the explosion emplacements or detonations. We believe that the explosive gases venting from the chamber into the tunnel complex, while certainly an asymmetric effect, would not strongly effect first arrivals and peaks at the three accelerometers.

Table 3.5 shows the rotated peak values of the in-plane radial (r) and tangential (t) velocity components together with the y component and the magnitude of the peak velocity vector for Tests 3, 4a, and 4b. In general, the radial peak velocities are only slightly smaller than the peak velocity magnitudes. We note again that for Test 4b only, gauges V1 and V2 have defective z-channels and V3 has defective a y-channel. Thus, only t and r components are computed at V3.

**Table 3.5.** Values of in-plane radial, r, in-plane tangential, t, and y components of peak particle velocity for Tests 3, 4a, and 4b in 1000 $m^3$ chamber. Positive t velocity is counterclockwise from (upward) direction.

| Test # Gauge # | Peak of r component (cm/s) | Peak of t component (cm/s) | Peak of y component (cm/s) | Magnitude of peak velocity (cm/s) |
|---|---|---|---|---|
| **Test 3** | | | | |
| **10 tons TNT** | | | | |
| V1 | 46.5 | -7 | 16.4 | 49.8 |
| V2 | 15.6 | -3.9 | 3.1 | 16.4 |
| V3 | 9.7 | 2.7 | -0.64 | 10.1 |
| **Test 4a** | | | | |
| **2.5 tons TNT** | | | | |
| V1 | 11 | -1.2 | 4.2 | 11.8 |
| V2 | 3.5 | -0.7 | 0.7 | 3.6 |
| V3 | 1.7 | 0.3 | 0 | 1.7 |
| **Test 4b** | | | | |
| **10 tons Ammo** | | | | |
| V1 | N/A | N/A | 7.2 | N/A |
| V2 | N/A | N/A | 1.5 | N/A |
| V3 | 6.0 | 1.5 | N/A | N/A |

N/A indicates defective channels involved

In the absence of the large, unexpected y components, the values of the in-plane tangential component of peak velocity may be considered a measure of the physical effect of the non-sphericity of the test chamber and explosive emplacement. Using a point source argument, this non-spherical effect would be expected to be largest for the closest gauge, V1, and smallest for the furthest gauge from the chamber, V3. In fact, the Table 4 shows substantial tangential, t, components for all working gauges (10% or more of the radial component). At gauge V3 for all three tests, the tangential velocity is positive (counterclockwise from the upward direction), while at gauges V1 and V2 for Tests 3 and 4a, the tangential velocity is clockwise. We do not understand this change in direction of the tangential velocity. Note however that the magnitude of peak in-plane tangential motion, in many cases, is quite similar to the peak y component.

### 3.4.4 Spherically Symmetric Calculations

As a first step toward understanding these near field velocity measurements, we have performed spherically symmetric simulations for Tests 3 and 4a and compared the results with the observations. In these finite difference calculations, the long test chamber and axisymmetric explosive configurations were approximated as a spherical mass of TNT centered in a 1000 cubic meter spherical chamber of approximately 6.20 m. For Test 3, the 10,000 kg (10 metric tons) of TNT gave an outer radius of ~1.136 meters for the TNT, assuming normal TNT density of 1.63 $g/cm^3$. For Test 4a, the radius of the 2.5 ton TNT sphere was calculated to be ~0.7155 m.

The explosive was center detonated, with the propagation of the detonation wave through the TNT computed using the JWL equation of state. The JWL equation of state has been used to

accurately describe the pressure-volume-energy behavior of the detonation products of explosive in metal acceleration applications. The equation is (Lee et al., 1973)

$$P = A(1-\frac{\omega}{R_1 V})e^{-R_1 V} + B(1-\frac{\omega}{R_2 V})e^{-R_2 V} + \frac{\omega E}{V}$$

where P=pressure in Mb, E=energy density in Mb-cc/cc and V= (volume of detonation products)/(volume undetonated explosive). For pure TNT, the parameters are listed in Table 3.6.

**Table 3.6.** The experimental values for pure TNT parameters in the JWL equation

| Parameter | Value | Unit conversion |
|---|---|---|
| A | 3.712 MB | $3.712\times10^{12}\,dyn/cm^2$ |
| B | 0.03231 MB | $3.231\times10^{10}\,dyn/cm^2$ |
| C | 0.01045 MB | $1.045\times10^{10}\,dyn/cm^2$ |
| R1 | 4.15 | |
| R2 | 0.95 | |
| ω | 0.30 | |

The surrounding air was modeled using an equation of state for air originally developed by the Air Force Weapons Laboratory, which has subsequently been validated through many successful simulations at SAIC. The rock surrounding the test chamber was modeled as granite.

For the simulations shown here, a relatively simple model was used to describe the rock behavior. This granite model (YF-AF, Stevens et al., 2002) presumed an elastic response coupled to a non-associated radial return flow rule with a failure surface based on that measured in the laboratory on fractured granite cores from the Piledriver test site. Elastic constants used were a bulk modulus of 483 kb, a shear modulus of 207 kb, and a density of 2.60 g/cm$^3$.

Figure 3.16 shows the radial particle velocities calculated at the radial ranges of the three gauge locations (V1, V2, and V3) from Tests 3 and 4a. The dashed particle velocities are the gauge measurements rotated into the in-plane radial direction as discussed above. Comparisons between simulated and measured particle velocities in the first signals, except for the arrival times, are fairly good. Note that the calculated subsequent signals represent reverberations in a spherical cavity and should not be expected to agree well with the measurements from these tests in a long chamber.

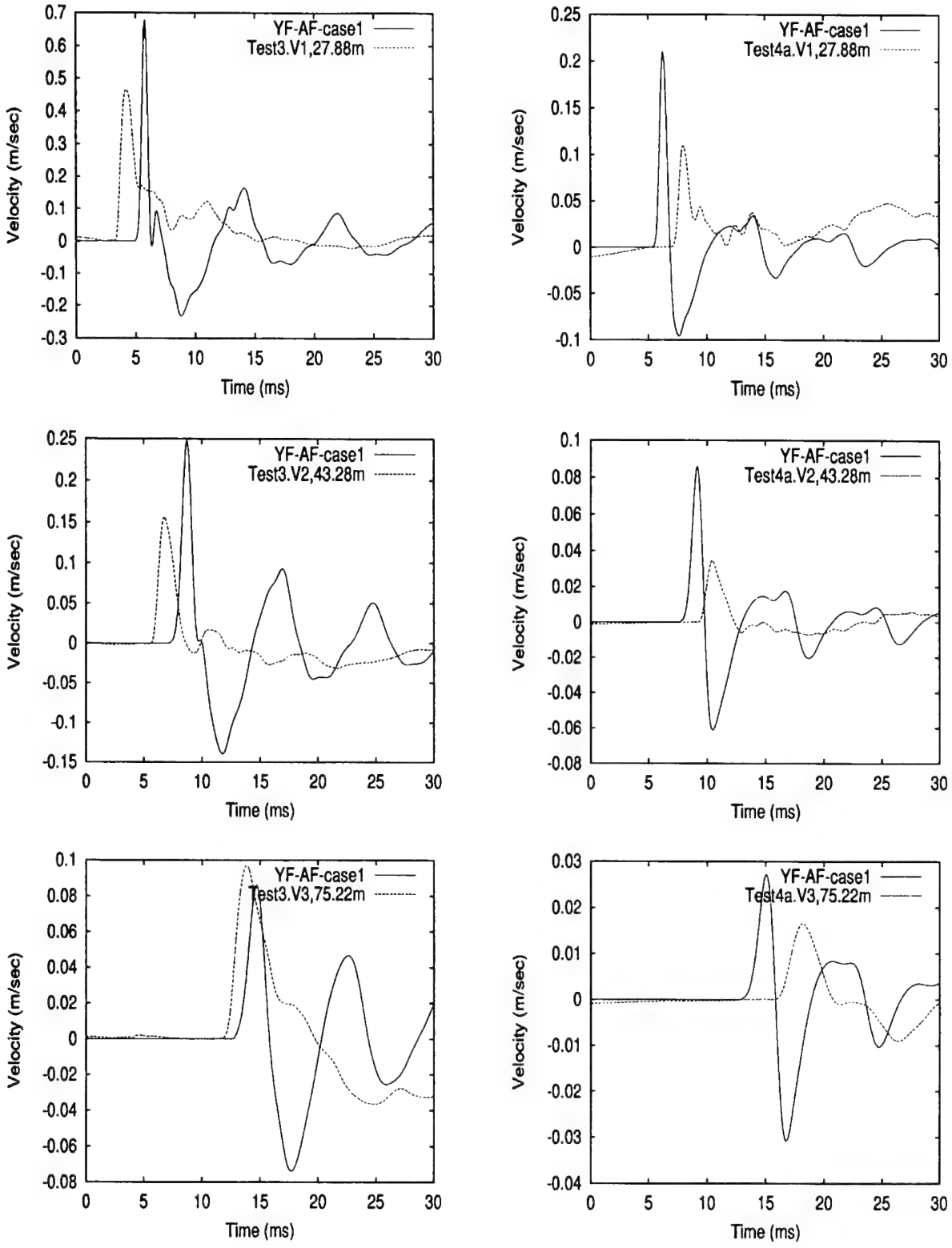


**Figure 3.16.** Radial particle velocities from a spherically symmetric simulation of Test 3 (10tons, left) and Test 4a (2.5 tons, right). Measurements at gauges V1, V2, and V3 are shown as dashed lines.

Figure 3.17 shows the velocity data and spherical calculation scaled to correspond approximately to the same yield. Using cube root scaling, increasing the yield by a factor of four leads to the same waveforms with all dimensions and the time scale increased by a factor of $4^{1/3}$. So the velocity waveform from a 2.5 ton explosion recorded at a distance of gauge V1 (27.7 m) and the time scale increased by that factor should be approximately the same as the velocity waveform from the 10 ton explosion at the distance of gauge V2 (43.1 m). Scaling does not work exactly because the chamber volume remains the same in the two cases. Nevertheless, it is useful for comparison. Figure 3.17 shows that both the data and the calculation for the 10 ton case are larger than the scaled 2.5 ton case, and the difference indicates the increase in coupling due to nonlinear deformation from the larger explosion. The calculated waveforms at this location are larger than the observations. As discussed in the following section on 3D calculations, this is due to the location of the gauges off the long end of the chamber.

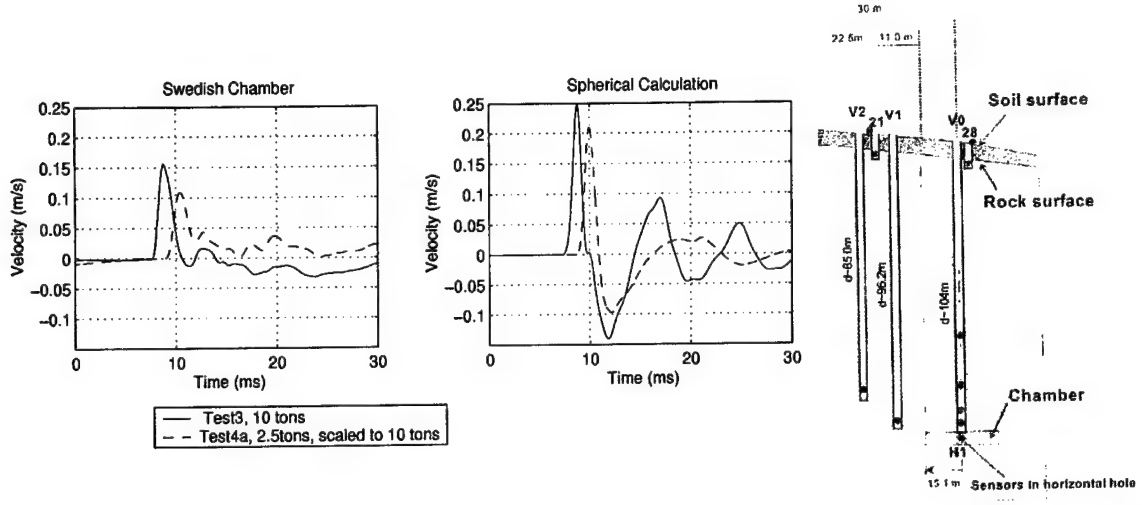


**Figure 3.17.** Red lines show the 10 ton chamber data and the spherical calculation at gauge V2. Blue lines show the 2.5 ton data and calculation at gauge V1, scaled to 10 tons (by increasing time scale by $4^{1/3}$) which is approximately equivalent to recording at V2. Coupling predicted from the spherical calculation is larger than the data at this location. The geometry of the gauges is shown on the right.

Figure 3.18 shows a comparison between the "observed" decoupling factors for the Swedish explosions and decoupling factors for a series of calculations of chemical explosions in a cavity in granite. "Observed" is in quotes because we do not have data from a tamped explosion for comparison. Instead, we scaled the decoupling factor of the most decoupled explosion to 100 to agree with the calculation for a fully decoupled explosion. The figure shows that the explosions remain almost fully decoupled until the charge/volume is approximately equal to 10, after which increases in yield cause a rapid decrease in decoupling. The calculation also shows this effect of nearly constant decoupling followed by a rapid decline. In the calculation the decline occurs at a higher charge/volume, most likely because the Swedish cavities are not spherical, which increases coupling. We investigate this further with 3D calculations in the next section of this report.

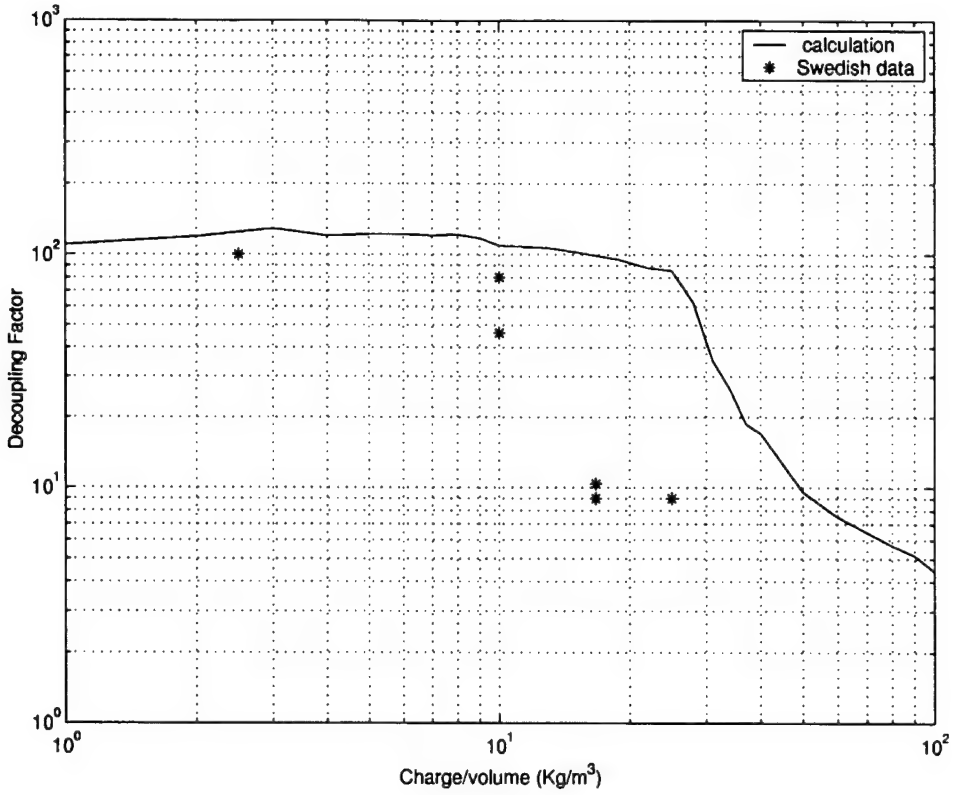


**Figure 3.18.** Observed and predicted decoupling factor for Swedish explosions. Calculations were for a chemical explosion in a 6.3 meter spherical cavity in hard (non-weakening) granite. The decoupling factor contains an unknown scale factor. The horizontal axis corresponds approximately to the overdrive factor above full decoupling.

### 3.4.5 Three-Dimensional Calculations

In order to increase our understanding of the Swedish chamber explosions, several three-dimensional finite difference calculations were performed using the "Stellar" code. Stellar is a second-order accurate Eulerian two- and three-dimensional stress wave propagation code with the same constitutive models that were used for the spherically symmetric calculations. The chamber was modeled as an air-filled chamber with dimensions 4.8m high (x axis), 30m long (y axis), and 7.2m wide (z axis). The near field results are sensitive to the layout of the explosive in the chamber, so several layouts were used in the simulations. The grid is shown in Figure 3.19. All calculations were performed in a 1/8 space, taking advantage of symmetry across the three planes through the center of the rectangular chamber. In this first calculation, the finite difference grid was 20m x 30m x 20m in size, with 100x100x100 grid blocks. The chamber is 2.4m x 15m x 3.6m. The explosive was placed in a flat layer along the x=0 plane, with a dimension of 0.2m x 2.7m x 0.8m, with a total energy of 1.25 tons. Note that all because of symmetry, all linear dimensions are effectively multiplied by two and volumes by eight, so this is equivalent to a 10 ton explosion in the chamber described earlier.

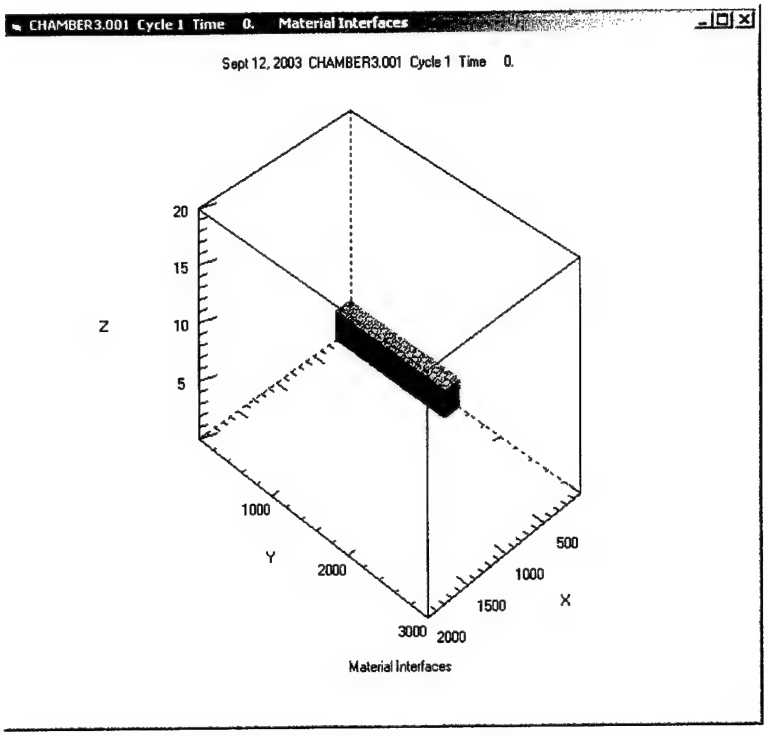


**Figure 3.19.** Geometry of grid used in one of the 3D calculations. The rectangle in the center is the chamber. There is symmetry about all three axes. Units of X, Y axes are in cm, Z is in meters.

The series of images in Figure 3.20 shows the evolution of the pressure field in the x-y plane near z=0 as a function of time in the calculation. The images show the initial high pressure field immediately after detonation, the propagation of the shock into the surrounding chamber wall, the propagation of the wave down the long axis of the chamber, a secondary high pressure region as the shock hits the end of the chamber, and initiation of the pressure wave that propagates out of the nonlinear region that later becomes visible as a seismic signal. The region closest to the explosion is hit hardest and a residual pressure due to nonlinear deformation remains both here and at the end of the chamber. A second calculation was performed with the same geometry, except that the explosive was reduced to an area of 0.2m x 2.7m x 0.2m, corresponding to a total energy (including symmetric regions) of 2.5 tons. Figure 3.21 shows a comparison of the regions of nonlinear deformation for these two calculations.

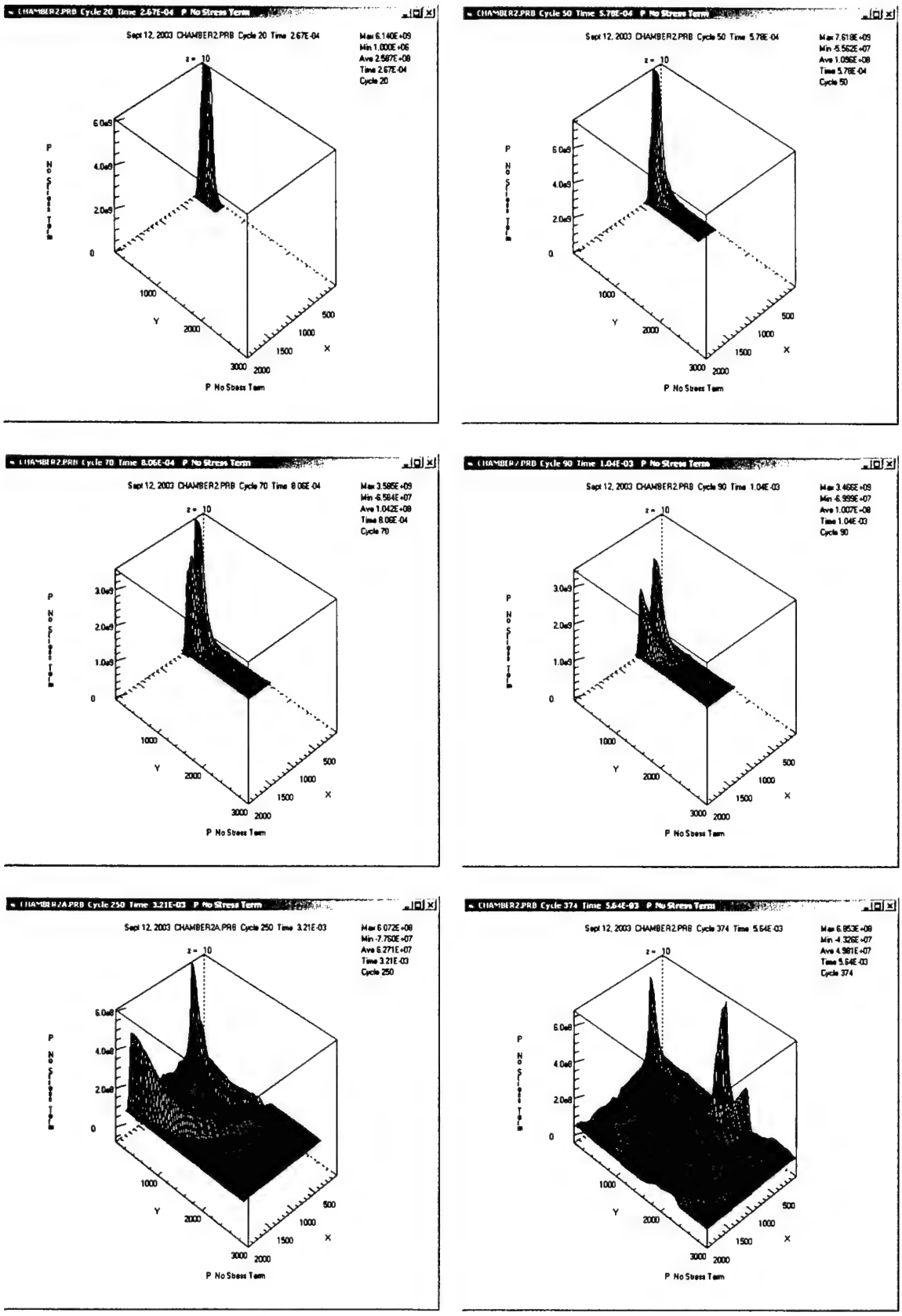


**Figure 3.20.** Pressure from 3D chamber calculation at times of 0.27, 0.58, 0.8, 1.0, 3.2 and 5.6 msec.

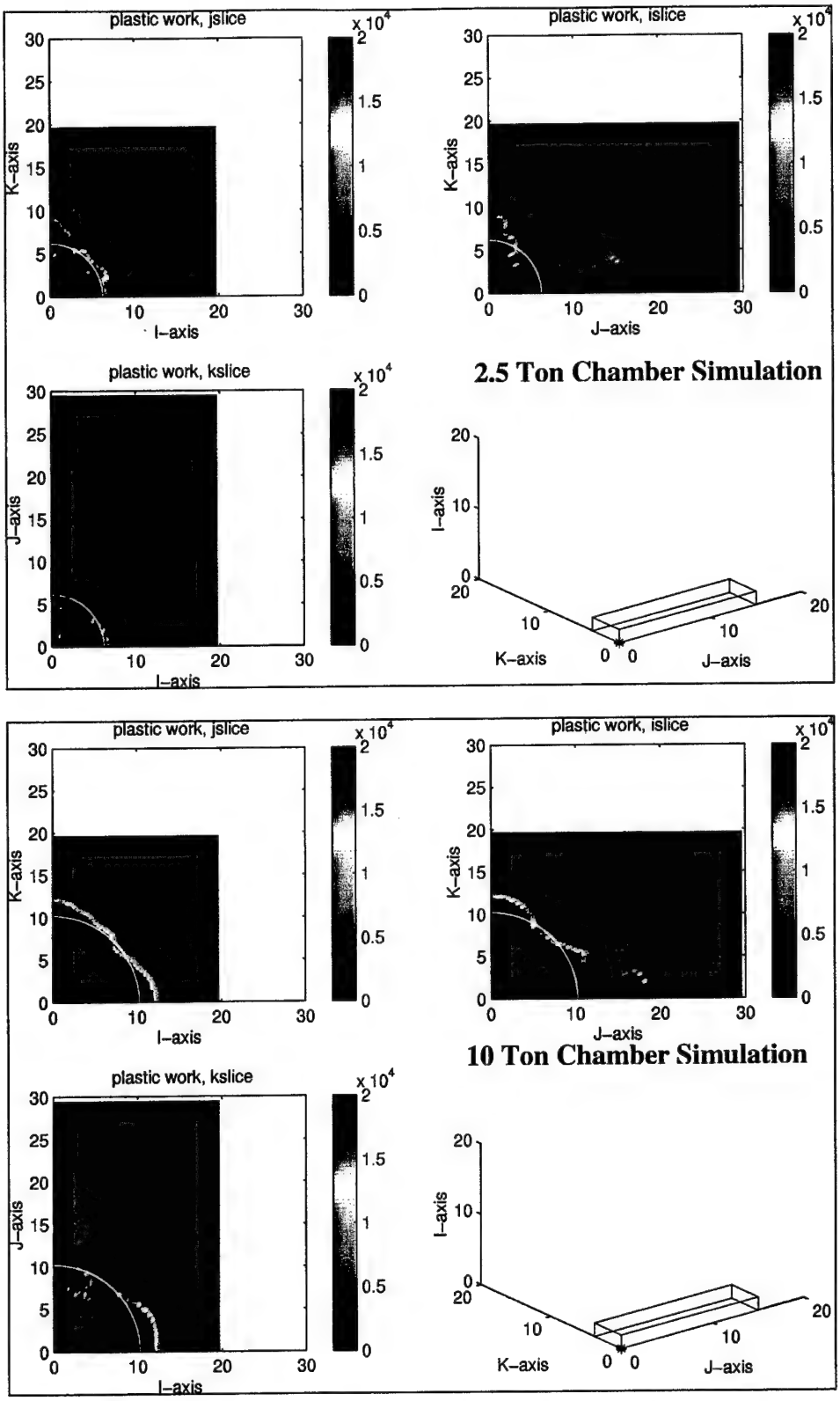


**Figure 3.21.** Regions of nonlinear deformation for 2.5 ton chamber calculation (top) and the 10 ton chamber calculation (bottom). The three figures show the nonlinear deformation around each of the three axes. The yellow line is the region of nonlinear deformation for an equivalent volume sphere.

A third set of calculations (Figure 3.22a,b) was performed with an improved model for the explosive, and a layout more consistent with the actual layout of explosives, which was set out in a series of small pads dispersed over a larger part of the chamber. We model this in the simulation as two pads which by symmetry corresponds to 8 pads each of twice the thickness used in the calculation. The result is two strong initial pulses, and a more complicated state within the chamber, but a somewhat reduced effect on the chamber wall. Note also the radiation pattern of the outgoing wave, with a stronger pressure in the direction along the narrowest dimension of the chamber, and reduced amplitudes along the long axis of the chamber.

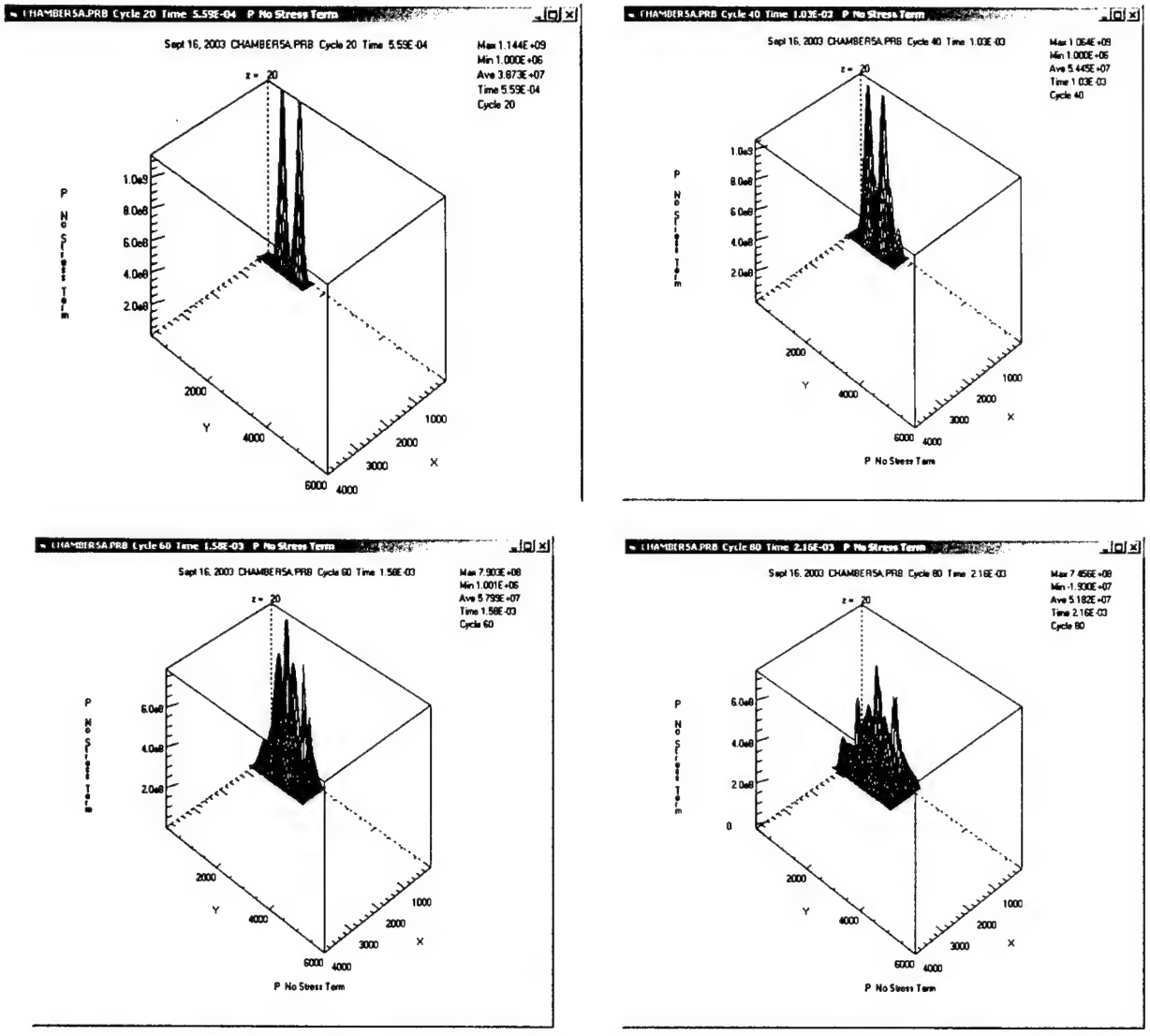


**Figure 3.22a.** Pressure from 3D chamber calculation with better explosive representation at times of 0.6, 1.0, 1.6, and 2.2 msec.

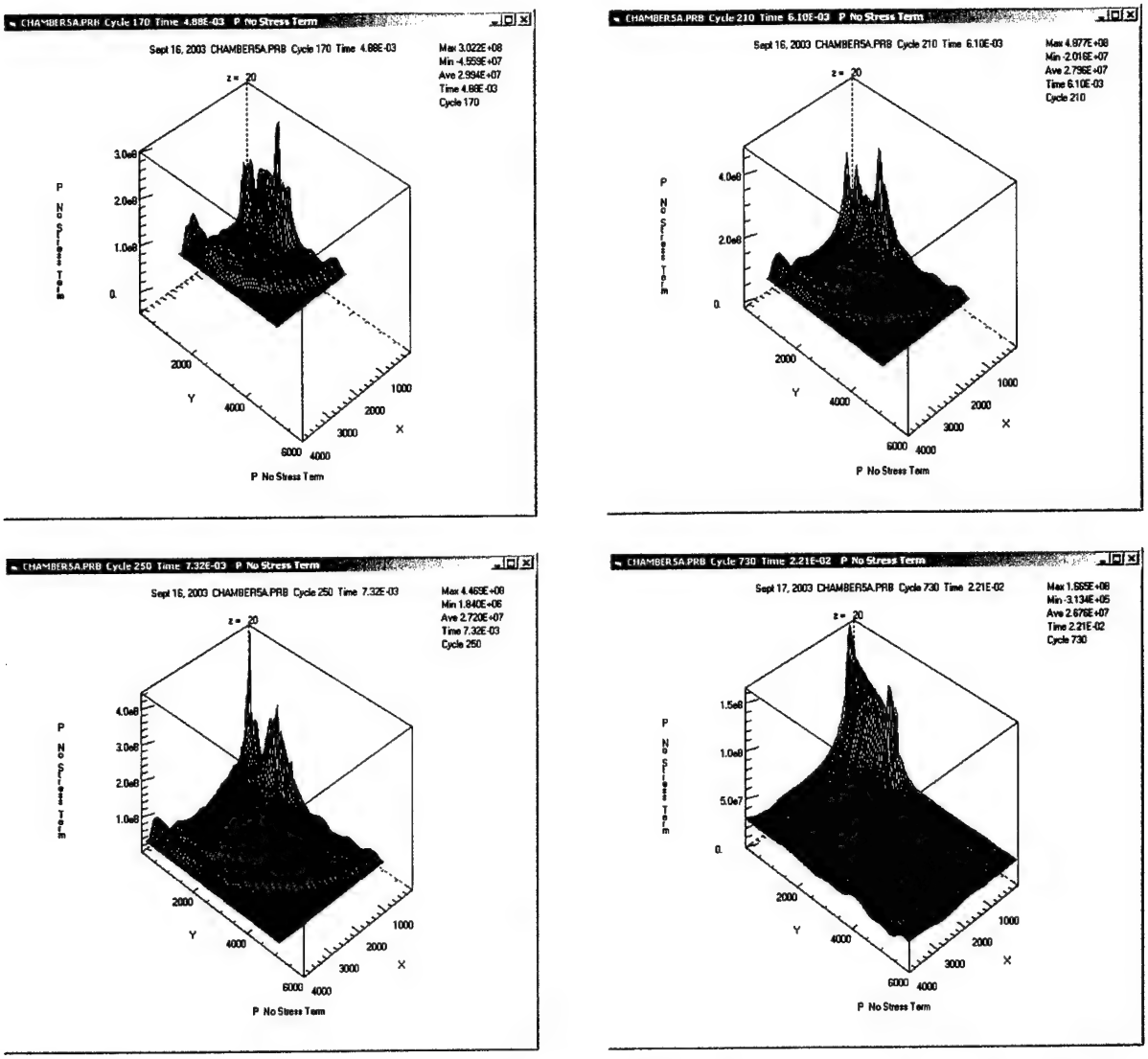


**Figure 3.22b.** Pressure from 3D chamber calculation with better explosive representation at times of 4.9. 6.1, 7.3 and 22 msec.

Figure 3.23 shows that calculated waveforms at the locations of recording stations V1 and V2, together with the horizontal and vertical components of the recorded waveforms at the same locations. As with the spherical calculations, the chamber reverberations are stronger than the observations, however the peak amplitudes and general shape and duration of the waveforms are reproduced fairly well. As noted above, there is a strong radiation pattern to the waveforms, with stronger amplitudes above and below the chamber and reduced amplitudes along the long axis of the chamber near the recording points V1 and V2.

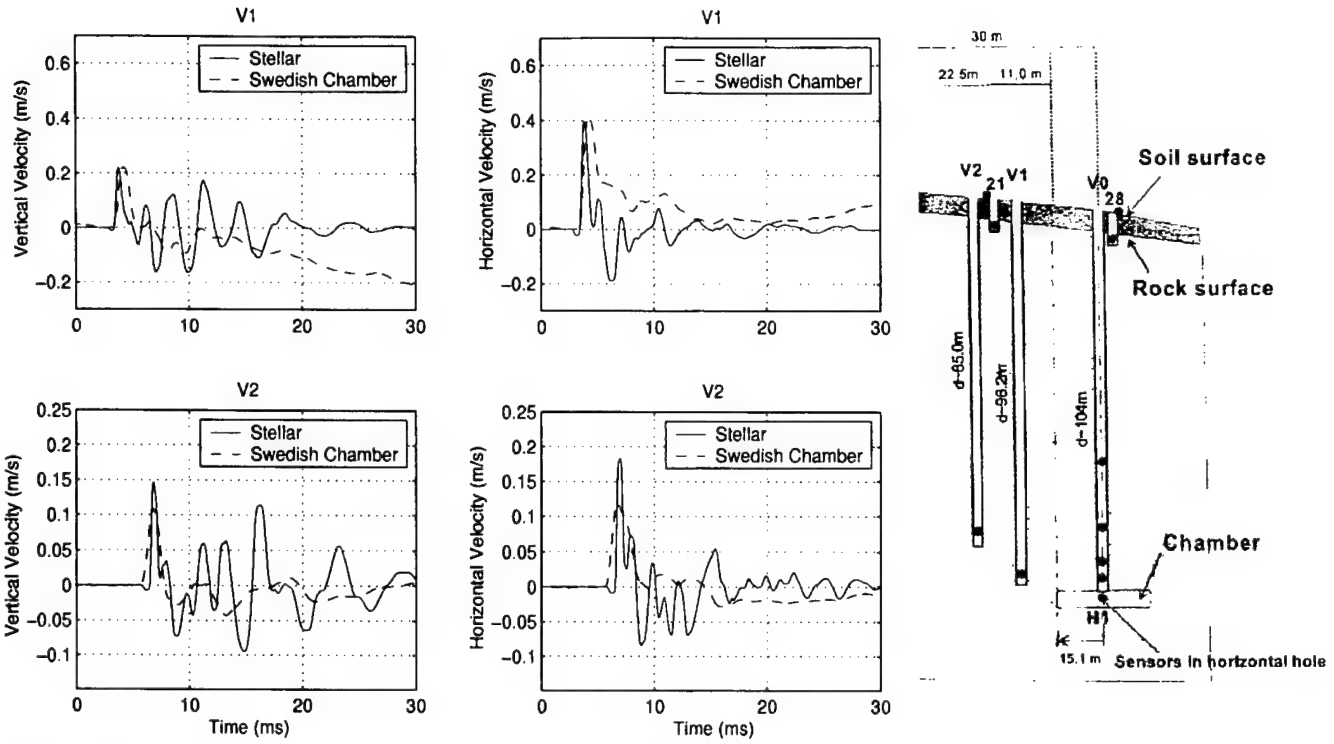


**Figure 3.23.** Data and calculated waveforms at stations V1 and V2. The station geometry relative to the chamber is shown on the right.

# 4. KIRGHIZIA DECOUPLED CHEMICAL EXPLOSIONS

During the summer of 1960, Soviet scientists carried out a series of HE cavity decoupling tests in a mine in the Tywya Mountains of Kirghizia. This program included tests designed to evaluate the effects of cavity shape and charge geometry on decoupling effectiveness, in addition to conventional spherical cavity tests similar to those employed in the corresponding U.S. COWBOY test series. The Kirghizia test series was composed of 10 tamped and 12 decoupled explosions with yields of 0.1, 1.0 and 6.0 tons. For the cavity tests the explosives were suspended in the chambers and included cases in which the explosives were positioned off center, near the cavity walls. The configurations of the various cavity tests are graphically summarized in Figure 4.1 for each of the five test chambers.

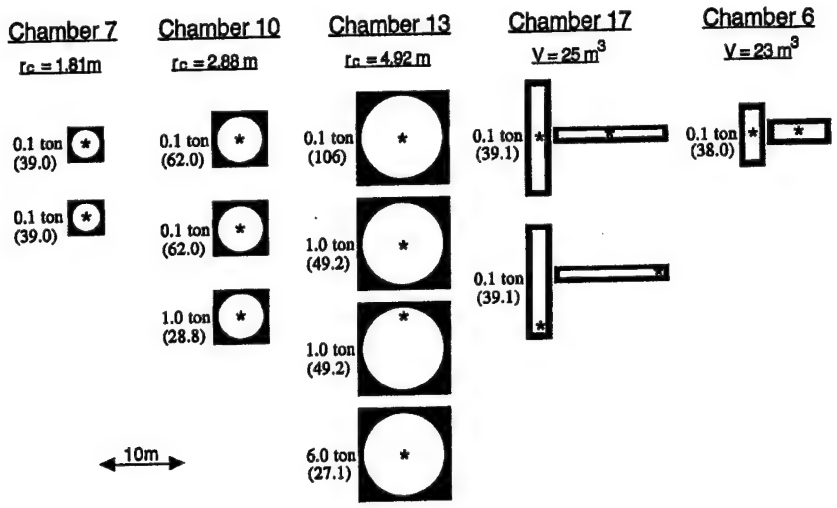


**Figure 4.1.** Graphical summary of the Kirghizia HE decoupling tests conducted in each of the excavated explosion chambers. The asterisk denotes the emplacement location of the charge within the chamber for each test. For the nonspherical cases, both horizontal (left) and vertical (right) sections through the chambers are displayed. The numerical values shown in parentheses below the yield values are the scaled radii in $m/kt^{1/3}$, with equivalent volume spherical cavity values listed for the nonspherical cases.

In our previous analysis of these tests (Murphy et al, 1997), we focused on free-field data recorded in the mine at distances on the order of 10 – 200 m. Unfortunately, only limited waveform data were available from this regime and, consequently, the analyses focused primarily on comparisons of peak amplitude values. While such comparisons provided a reasonable basis for comparing the relative decoupling effectiveness of different cavity configurations, they did not provide an adequate data set for confidently determining the frequency dependence of the absolute level of the decoupling factor. Consequently, under the current effort, we have recovered and digitized seismic data from these tests recorded at surface stations located at distances of 5 and 10 km. High quality recordings are available from the 1 ton tamped and decoupled tests at the 5 km station, and the 6 ton tamped and decoupled tests at the 10 km station. Results of detailed analyses of these data have proven to be generally quite consistent with those obtained from the previous analysis of the corresponding free-field data. Examples of these data are shown in Figure 4.2 which provides a comparison of vertical component recordings at the 5 km station from 1 ton tamped and decoupled explosions. In this

case, the decoupled tests were conducted at the center of spherical cavities with radii of 4.92 and 2.88 m, and 1 m from the wall of the 4.92 radius cavity. It can be seen that the signal levels for the tests in the centers of the two different sized cavities are very comparable, indicating peak motion decoupling factors of about 20 and suggesting that both of these tests in different size cavities were fully decoupled. The signal level for the test near the cavity wall is about a factor of 2 larger, suggesting some significantly enhanced coupling associated with local nonlinear wall response.

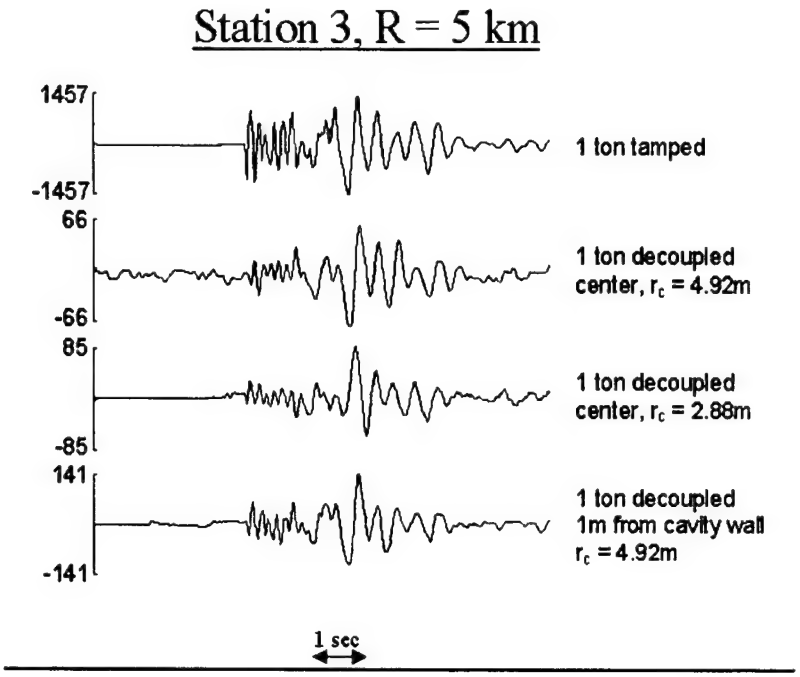


**Figure 4.2.** Vertical component recordings at the 5 km surface station from 1 ton tamped and decoupled explosions.

Recordings from the 6 ton tamped and decoupled explosions at the 10 km station are shown in Figure 4.3. In this case the decoupled explosion was detonated at the center of the 4.92 m radius spherical cavity. Again, the peak signal levels from the two tests shows a decoupling factor of a little more than 20, consistent with the results from the 5 km station and suggesting that this larger test was also fully decoupled . We have computed frequency-dependent decoupling factors between 1 and 4 Hz from these 5 and 10 km station recordings and the results are shown in Figure 4.4, where it can be seen that the decoupling factors for the two 1 ton tests in the centers of the different sized cavities over this frequency band are essentially identical and consistent with a low frequency decoupling factor in the range 20 - 30. This confirms that these explosions must have been essentially fully decoupled. The frequency dependent decoupling factor for the 1 ton test near the cavity wall is quite similar to the other two in shape, but lower by about a factor of 2, independent of frequency over this range. The results from the 6 ton test are in good agreement with those of the fully decoupled 1 ton tests, suggesting that it also was essentially fully decoupled. The decoupling factor for all of these fully decoupled tests over this frequency band is somewhere in the range of about 20 to 30. Also shown on this figure are the corresponding results at higher frequency (i.e. 10 – 200 Hz) obtained previously by Murphy et al (1997) using the limited free-field waveform data. It can be seen that the results from the two distance regimes are generally quite consistent, confirming a low frequency decoupling factor in the range of 20 – 30 for these fully decoupled tests in limestone.

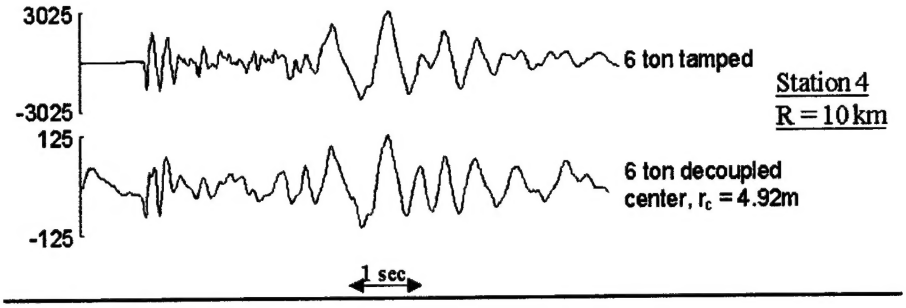


**Figure 4.3.** Vertical component recordings from the 6 ton tamped and decoupled tests at the 10 km station.

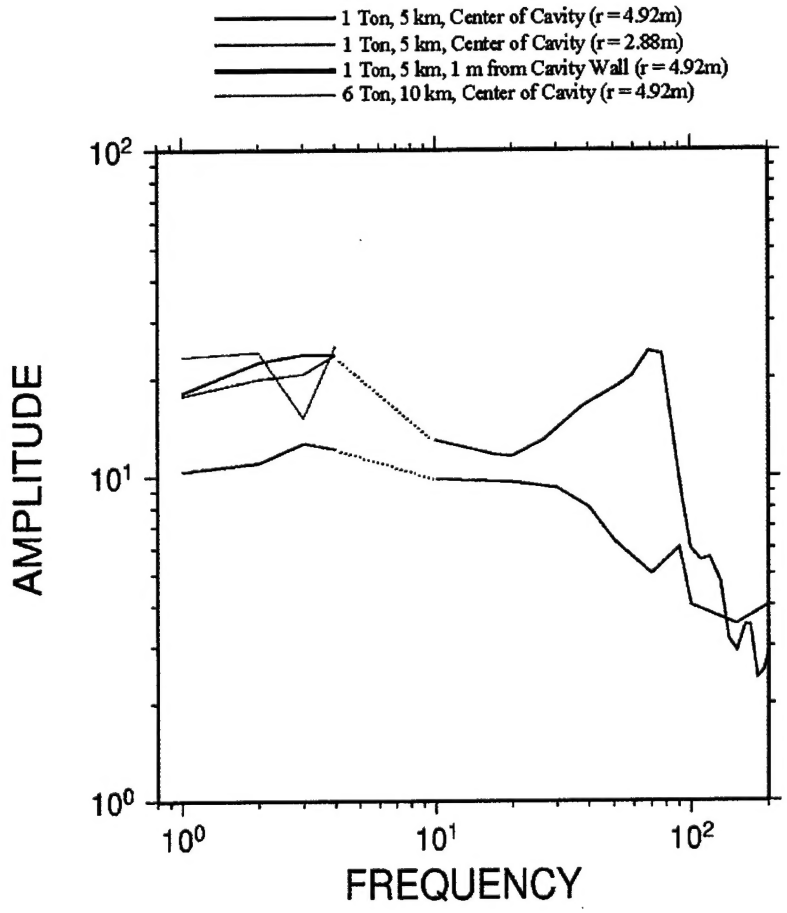


**Figure 4.4.** Frequency dependent decoupling factors for the 1 and 6 ton tests at the 5 and 10 km stations. Also shown are the corresponding results at higher frequency (i.e. 10 – 200 Hz) obtained previously by Murphy et al (1997) from the corresponding free-field data.

## 5. CONCLUSIONS AND RECOMMENDATIONS

We are in the second year of a project to evaluate the decoupling effectiveness of underground cavities in a variety of configurations. New data sets have been provided by NORSAR and IDG that help to constrain the problem, particularly for the important partially coupled regime. Following is a summary of our results to date:

- Kirghizia Mine explosions provided by IDG:
    - New data recorded on the surface at distances of 5 and 10 km have been analyzed and the results have been found to be generally consistent with previous results obtained from more limited free-field data, confirming low frequency decoupling factors in the range of 20-30 for fully decoupled HE tests in limestone.
    - An explosion close to a cavity wall increases coupling by about a factor of 2.
    - Decoupling in this data set is insensitive to cavity shape.
- Swedish decoupled explosions provided by NORSAR:
    - A fully decoupled 2.5 ton explosion is detectable at NORSAR at a distance of 140 km.
    - This data set covers a range of yields overdriven beyond full decoupling by factors of approximately 2-25.
    - Decoupling remains approximately complete for yields less than 10 times the Latter decoupling criterion.
    - At higher yields coupling increases rapidly, increasing by an order of magnitude for a factor of 2 increase in yield/volume.
    - 3D nonlinear calculations of the chamber explosions show strong nonlinearity at the points closest to the explosion. For the 10 ton explosion the total nonlinear volume is only slightly greater than a spherical explosion of the same volume.

## REFERENCES


Gronsten, G. A. (2000), "The Älvdalen Large Scale Tests", Data report from the Norwegian measurements, Fortifikatorisk notat nr. 286/01, Forsvarets Bygningstjeneste, Oslo, Norway, 2000.

Gronsten, G. A. and Krest, O. (2002), "The Älvdalen Large Scale Tests", Data report from the Norwegian measurements, Fortifikatorisk notat nr. 297/01, Forsvarets Bygningstjeneste, Oslo, Norway, 2001.

Herbst, R. F., G. C., Werth and D. L. Springer (1961), "Use of Large Cavities to Reduce Seismic Waves From Underground Explosions," J. Geophys. Res., 66, p. 959.

Kitov, I. O., D. D. Sultanov, V. V. Adushkin, V. N. Kostuchenko, O. P. Kuznetsov, P. B. Kaazik, N. I. Nedoshivin, H. D. Rubinshtein (1995), "Analysis of the Seismic Characteristics of U.S. and Russian Coupled and Cavity Decoupled Explosions in Salt," Institute for the Dynamics of the Geospheres, Final Report 911412, August.

Lee, E., M. Finger and W. Collins, (1973), "JWL equation of state coefficients for high explosives," Lawrence Livermore Laboratory UCID-16189, Jan, 16.

Murphy, J. R., I. O. Kitov, N. Rimer, V. V. Adushkin and B. W. Barker (1997), "Seismic Characteristics of Cavity Decoupled Explosions in Limestone: An Analysis of Soviet High Explosive Test Data," Journal of Geophysical Research, 102, B12, pp. 27, 393-27, 405.

Stevens, J. L., J. R. Murphy and N. Rimer (1991), "Seismic Source Characteristics of Cavity Decoupled Explosions in Salt and Tuff," Bull. Seism. Soc. Am., 81, pp. 1272-1291.

Stevens, J. L., N. Rimer, H. Xu, G. E. Baker and S. M. Day (2003), "Near field and regional modeling of explosions at the Degelen Test Site," SAIC final report to DTRA, SAIC-02/2050, January.

Stevens, Jeffry L., Norton Rimer, Heming Xu, G. Eli Baker, John R. Murphy, Brian W. Barker, Conrad Lindholm, Frode Ringdal, Steven Gibbons, Tormod Kvaerna and Ivan Kitov (2002), "Analysis and Simulation of Cavity-Decoupled Chemical Explosions," SAIC Annual Report No. 1 submitted to the Defense Threat Reduction Agency, SAIC-02/2046, October.